

# 1 Nitrogen Fixation in Arctic Coastal Waters (Qeqertarsuaq, West 2 Greenland): Influence of Glacial Melt on Diazotrophs, Nutrient 3 Availability, and Seasonal Blooms

4 Schlangen Isabell<sup>1</sup>, Leon-Palmero Elizabeth<sup>1,2</sup>, Moser Annabell<sup>1</sup>, Xu Peihang<sup>1</sup>, Laursen Erik<sup>1</sup>, and  
5 Löscher Carolin R.<sup>1,3</sup>

6 <sup>1</sup>Nordceee, Department of Biology, University of Southern Denmark, Campusvej 55, 5230 Odense M, Denmark

7 <sup>2</sup>Department of Geosciences, Princeton University, Princeton, New Jersey

8 <sup>3</sup>DIAS, University of Southern Denmark, Odense, Denmark

9 **Correspondence:** Carolin R. Löscher (cloescher@biology.sdu.dk)

10  
11 **Abstract.** The Arctic Ocean is undergoing rapid transformation due to climate change, with decreasing sea ice contributing  
12 to a predicted increase in primary productivity. A critical factor determining future productivity in this region is the  
13 availability of nitrogen, a key nutrient that often limits biological growth in Arctic waters. The fixation of dinitrogen (N<sub>2</sub>)  
14 gas, a biological process mediated by diazotrophs, provides a source of new nitrogen to marine ecosystems and has been  
15 increasingly recognized as a potential contributor to nitrogen supply in the Arctic Ocean. Historically it was believed to be  
16 limited to oligotrophic tropical and subtropical oceans, Arctic N<sub>2</sub> fixation has only garnered significant attention over the  
17 past decade, leaving a gap in our understanding of its magnitude, the diazotrophic community, and potential environmental  
18 drivers. In this study, we investigated N<sub>2</sub> fixation rates and the diazotrophic community in Arctic coastal waters, using a  
19 combination of isotope labeling, genetic analyses and biogeochemical profiling, in order to explore its response to glacial  
20 meltwater, nutrient availability and its impact on primary productivity. We observed N<sub>2</sub> fixation rates ranging from 0.16 to  
21 2.71 nmol N L<sup>-1</sup> d<sup>-1</sup>, notably higher than many previously reported rates for Arctic waters. The diazotrophic community was  
22 predominantly composed of UCYN-A. The highest N<sub>2</sub> fixation rates co-occurred with peaks in chlorophyll *a* and primary  
23 production at a station in the Vaigat Strait, likely influenced by glacial meltwater input. On average, N<sub>2</sub> fixation contributed  
24 1.6% of the estimated nitrogen requirement of primary production, indicating that while its role is modest, it may still represent a  
25 nitrogen source in certain conditions. These findings illustrate the potential importance of N<sub>2</sub> fixation in an environment  
26 previously not considered important for this process and provide insights into its response to the projected melting of the  
27 polar ice cover.

## 28 29 **1 Introduction**

30  
31 Nitrogen is a key element for life and often acts as a growth-limiting factor for primary productivity (Gruber and Sarmiento,  
32 1997; Gruber, 2004; Gruber and Galloway, 2008). Despite nitrogen gas (N<sub>2</sub>) making up approximately 78% of the  
33 atmosphere, it remains inaccessible to most marine life forms. Diazotrophs, which are specialized bacteria and archaea,  
34 have the ability to convert N<sub>2</sub> into biologically available nitrogen, facilitated by the nitrogenase enzyme complex carrying

35 out the process of

36 biological nitrogen fixation ( $N_2$  fixation) (Capone and Carpenter (1982)). Despite the fact that these organisms are highly  
37 specialized and  $N_2$  fixation is energetically demanding, the ability to carry out this process is widespread amongst  
38 prokaryotes. However, it is controlled by several factors such as temperature, light, nutrients and trace metals such as iron  
39 and molybdenum (Sohm et al., 2011; Tang et al., 2019). Oceanic  $N_2$  fixation is the major source of nitrogen to the marine  
40 system (Karl et al., 2002; Gruber and Sarmiento, 1997), thus, diazotrophs determine the biological productivity of our  
41 planet (Falkowski et al. (2008), impact the global carbon cycle and the formation of organic matter (Galloway et al., 2004;  
42 Zehr and Capone, 2020). Traditionally it has been believed that the distribution of diazotrophs was limited to warm and  
43 oligotrophic waters (Buchanan et al., 2019; Sohm et al., 2011; Luo et al., 2012) until putative diazotrophs were identified  
44 in the central Arctic Ocean and Baffin Bay (Farnelid et al., 2011; Damm et al., 2010). First rate measurements have been  
45 reported for the Canadian Arctic by Blais et al. (2012) and recent studies have reported rate measurements in adjacent seas  
46 (Harding et al., 2018; Sipler et al., 2017; Shiozaki et al., 2017, 2018), drawing attention to cold and temperate waters as  
47 significant contributors to the global nitrogen budget through diverse organisms.

48 UCYN-A has been described as the dominant active  $N_2$  fixing cyanobacterial diazotroph in arctic waters (Harding et al.  
49 (2018)), while other cyanobacteria have only occasionally been reported (Díez et al., 2012; Fernández-Méndez et al., 2016;  
50 Blais et al.). However, other recent studies suggest, that the majority of the arctic marine diazotrophs are NCDs (non-  
51 cyanobacterial diazotroph) and those may contribute significantly to  $N_2$  fixation in the Arctic Ocean (Shiozaki et al., 2018;  
52 Fernández-Méndez et al., 2016; Harding et al., 2018; Von Friesen and Rie-mann, 2020). Recent work by Robicheau et al.  
53 (2023) nearby Baffin Bay, geographically close to the sampling area, document low *nifH* gene abundance while still detecting  
54 diazotrophs in Arctic surface waters, highlighting the patchy distribution of diazotrophs across Arctic coastal environments. Studies  
55 on the Arctic diazotroph community remain scarce, leaving Arctic environments poorly understood regarding  $N_2$  fixation.  
56 Shao et al. (2023) note the impossibility of estimating Arctic  $N_2$  fixation rates due to the sparse spatial coverage, which  
57 currently represents only approximately 1 % of the Arctic Ocean. Increasing data coverage in future studies will aid in  
58 better constraining the contribution of  $N_2$  fixation to the global oceanic nitrogen budget (Tang et al. (2019)).

59 The Arctic ecosystem is undergoing significant changes driven by rising temperatures and the accelerated melting of sea ice,  
60 a trend predicted to intensify in the future (Arrigo et al., 2008; Hanna et al., 2008; Haine et al., 2015). These climate-driven  
61 shifts have stimulated primary productivity in the Arctic by 57 % from 1998 to 2018, elevating nutrient demands in the  
62 Arctic Ocean (Ardyna and Arrigo, 2020; Arrigo and van Dijken, 2015; Lewis et al., 2020). This increase is attributed to  
63 prolonged phytoplankton growing seasons and expanding ice-free areas suitable for phytoplankton growth (Arrigo et al.  
64 (2008)). However, despite these dramatic changes, the role of  $N_2$  fixation in sustaining Arctic primary production remains  
65 poorly understood. While recent studies suggest that diazotrophic activity may contribute to nitrogen inputs in polar regions  
66 (Sipler et al. (2017)), fundamental uncertainties remain regarding the extend, distribution and environmental drivers of  $N_2$   
67 Fixation in the Arctic Ocean. Specifically, it is unclear whether increased glacial meltwater input enhances or inhibits  $N_2$   
68 Fixation through changes in nutrient availability, stratification, and microbial community composition. Thus, the question

69 of whether nitrogen limitation will emerge as a key factor constraining Arctic primary production under future climate scenarios  
70 remains unresolved. In this study, we investigate the diversity of diazotrophic communities alongside in situ N<sub>2</sub> fixation  
71 rate measurements in Disko Bay (Qeqertarsuaq), a coastal Arctic system strongly influenced by glacial meltwater input. By linking  
72 environmental parameters to N<sub>2</sub> fixation dynamics, we aim to clarify the role of diazotrophs in Arctic nutrient cycling and  
73 assess their potential contribution to sustaining primary production in a changing Arctic. Understanding these processes is  
74 essential for refining biogeochemical models and predicting ecosystem responses to future climate change.

75 **2 Material and methods**

76 **2.1 Seawater sampling**

77 The research expedition was conducted from August 16 to 26 in 2022 aboard the Danish military vessel P540 within the  
78 waters of Qeqertarsuaq, located in the western region of Greenland (Kalaallit Nunaat). Discrete water samples were  
79 obtained using a 10 L Niskin bottle, manually lowered with a hand winch to five distinct depths (surface, 5, 25, 50, and  
80 100 m). A comprehensive sampling strategy was employed at 10 stations (Fig. 1), covering the surface to a depth of 100 m.  
81 The sampled parameters included water characteristics, such as nutrient concentrations, chl *a*, particulate organic carbon  
82 (POC) and nitrogen (PON), molecular samples for nucleic acid extractions (DNA), dissolved inorganic carbon (DIC) as  
83 well as CTD sensor data. At three selected stations (3,7,10) N<sub>2</sub> fixation and primary production rates were quantified  
84 through concurrent incubation experiments.

85 Samples for nutrient analysis, nitrate (NO<sub>3</sub><sup>-</sup>), nitrite (NO<sub>2</sub><sup>-</sup>) and phosphate (PO<sub>4</sub><sup>3-</sup>) were taken in triplicates, filtered  
86 through a 0.22  $\mu$ m syringe filter (Avantor VWR® Radnor, Pa, USA) and stored at -20 °C until further analysis.  
87 Concentrations were spectrophotometrically determined (Thermo Scientific, Genesys 1OS UV-VIS spectrophotometer)  
88 following the established protocols of Murphy and Riley (1962) for PO<sub>4</sub><sup>3-</sup>; García-Robledo et al. (2014) for NO<sub>3</sub><sup>-</sup> & NO<sub>2</sub><sup>-</sup>  
89 (detection limits: 0.01  $\mu$ mol L<sup>-1</sup> (NO<sub>3</sub><sup>-</sup>, NO<sub>2</sub><sup>-</sup>, and PO<sub>4</sub><sup>3-</sup>), 0.05  $\mu$ mol L<sup>-1</sup> (NH<sub>4</sub><sup>+</sup>)). Chl *a* samples were filtered onto 47 mm  
90  $\varnothing$  GF/F filters (GE Healthcare Life Sciences, Whatman, USA), placed into darkened 15 mL LightSafe centrifuge tubes  
91 (Merck, Rahway, NJ, USA) and were subsequently stored at -20 °C until further analysis. To determine the Chl *a*  
92 concentration, the samples were immersed in 8 mL of 90 % acetone overnight at 5 °C. Subsequently, 1 mL of the resulting  
93 solution was transferred to a 1.5 mL glass vial (Mikrolab Aarhus A/S, Aarhus, Denmark) the following day and subjected  
94 to analysis using the Trilogy® Fluorometer (Model #7200-00) equipped with a Chl *a* in vivo blue module (Model #7200-  
95 043, both Turner Designs, San Jose, CA, USA). Measurements of serial dilutions from a 4 mg L<sup>-1</sup> stock standard and 90 %  
96 acetone (serving as blank) were performed to calibrate the instrument. In addition, measurements of a solid-state secondary  
97 standard were performed every 10 samples. Water (1 L) from each depth was filtered for the determination of POC and  
98 PON concentrations, as well as natural isotope abundance ( $\delta$  <sup>13</sup>C POC /  $\delta$  <sup>15</sup>N PON) using 47 mm  $\varnothing$ , 0.7  $\mu$ m nominal pore  
99 size precombusted GF/F filter (GE Healthcare Life Sciences, Whatman, USA), which were subsequently stored at -20 °C  
100 until further analysis. Seawater samples for DNA were filtered through 47 mm  $\varnothing$ , 0.22  $\mu$ m MCE membrane filter (Merck,  
101 102 103 until further analysis.

104 Millipore Ltd., Ireland) for a maximum of 20 minutes, employing a gentle vacuum (200 mbar). The filtered volumes varied  
105 depending

106 on the amount of material captured on the filter, ranging from 1.3 L to 2 L, with precise measurements recorded. The filters  
107 were promptly stored at -20 °C on the ship and moved to -80 °C upon arrival to the lab until further analysis.

108 To achieve detailed vertical profiles, a conductivity-temperature-depth-profiler (CTD, Seabird X) equipped with  
109 supplementary sensors for dissolved oxygen (DO), photosynthetically active radiation (PAR), and fluorescence (Flurometer)  
110 was manually deployed.

## 111 **2.2 Nitrogen fixation and primary production**

112  
113 Water samples were collected at three distinct depths (0, 25 and 50 m) for the investigation of N<sub>2</sub> fixation rates and primary  
114 production rates, encompassing the euphotic zone, chlorophyll maximum, and a light-absent zone. Three incubation  
115 stations (Fig. 2: station 3, 7, 10) were chosen, in a way to cover the variability of the study area. This strategic sampling  
116 aimed to capture a gradient of the water column with varying environmental conditions, relevant to the aim of the study.  
117 N<sub>2</sub> fixation rates were assessed through triplicate incubations employing the modified <sup>15</sup>N-N<sub>2</sub> dissolution technique after  
118 Großkopf et al. (2012) and Mohr et al. (2010).

119 To ensure minimal contamination, 2.3 L glass bottles (Schott-Duran, Wertheim, Germany) underwent pre-cleaning and  
120 acid washing before being filled with seawater samples. Oxygen contamination during sample collection was mitigated by  
121 gently and bubble-free filling the bottles from the bottom, allowing the water to overflow. Each incubation bottle received  
122 a 100 mL amendment of <sup>15</sup>N-N<sub>2</sub> enriched seawater (98 %, Cambridge Isotope Laboratories, Inc., USA) achieving an average  
123 dissolved N<sub>2</sub> isotope abundance (<sup>15</sup>N atom %) of 3.90 ± 0.02 atom % (mean ± SD). Additionally, 1 mL of H<sup>13</sup>CO<sub>3</sub> (1g/50  
124 mL) (Sigma- Aldrich, Saint Louis Missouri US) was added to each incubation bottle, roughly corresponding to 10 atom %  
125 enrichment and thus measurements of primary production and N<sub>2</sub> fixation were conducted in the same bottle. Following  
126 the addition of both isotopic components, the bottles were closed airtight with septa-fitted caps and incubated for 24 hours  
127 on-deck incubators with a continuous surface seawater flow. These incubators, partially shaded (using daylight-filtering  
128 foil) to simulate in situ photosynthetically active radiation (PAR) conditions, aimed to replicate environmental parameters  
129 experienced at the sampled depths. Control incubations utilizing atmospheric air served as controls to monitor any natural  
130 changes in  $\delta$  <sup>15</sup>N not attributable to <sup>15</sup>N-N<sub>2</sub> addition. These control incubations were conducted using the dissolution  
131 method, like the <sup>15</sup>N-N<sub>2</sub> enrichment experiments, but with the substitution of atmospheric air instead of isotopic tracer.

132 After the incubation period, subsamples for nutrient analysis were taken from each incubation sample, and the remaining  
133 content was subjected to the filtration process and were gently filtered (200 mbar) onto precombusted GF/F filters  
134 (Advantec,

135 47 mm ø, 0.7  $\mu$ m nominal pore size). This step ensured a comprehensive examination of both nutrient dynamics and the  
136 isotopic composition of the particulate pool in the incubated samples. Samples were stored at -20 °C until further analysis.  
137 Upon arrival in the lab, the filters were dried at 60 °C and to eliminate particulate inorganic carbon, subsequently subject to

138 acid fuming during which they were exposed to concentrated hydrochloric acid (HCL) vapors overnight in a desiccator. After  
139 undergoing acid treatment, the filters were carefully dried, then placed into tin capsules and pelletized for subsequent analysis.  
140 The determination of POC and PON, as well as isotopic composition ( $\delta^{13}\text{C}$  POC /  $\delta^{15}\text{N}$  PON), was carried out using an  
141 elemental analyzer (Flash EA, ThermoFisher, USA) connected to a mass spectrometer (Delta V Advantage Isotope Ratio MS,  
142 ThermoFisher, USA) with the ConFlo IV interface. This analytical setup was applied to all filters. These values, derived from  
143 triplicate incubation measurements, exhibited no omission of data points or identification of outliers. Final rate calculations for  
144  $\text{N}_2$  fixation rates were performed after Mohr et al. (2010) and primary production rates after Slawyk et al. (1977). A detailed  
145 sensitivity analysis of  $\text{N}_2$  fixation rates, including the contribution of each source of error for all parameters, is provided in a  
146 supplementary table and summarized form in the Appendix (Table A1).

### 147 2.3 Molecular methods

148 The filters were flash-frozen in liquid nitrogen, crushed and DNA was extracted using the Qiagen DNA/RNA AllPrep Kit  
149 (Qiagen, Hildesheim, DE), following the procedure outlined by the manufacturer. The concentration and quality of the  
150 extracted DNA was assessed spectrophotometrically using a MySpec spectrofluorometer (VWR, Darmstadt, Germany).  
151 The preparation of the metagenome library and sequencing were performed by BGI (China). Sequencing libraries were  
152 generated using MGIEasy Fast FS DNA Library Prep Set following the manufacturer's protocol. Sequencing was  
153 conducted with 2x150bp on a DNBSEQ-G400 platform (MGI). SOAPnuke1.5.5 (Chen et al. (2018)) was used to filter and  
154 trim low quality reads and adaptor contaminants from the raw sequence reads, as clean reads. In total, fifteen metagenomic  
155 datasets were produced with an average of 9.6G bp per sample.  
156

#### 157 2.3.1 Metagenomic De Novo assembly, gene prediction, and annotation

158 Megahit v1.2.9 (Li et al. (2015)) was used to assemble clean reads for each dataset with its minimum contig length as 500.  
159 Prodigal v2.6.3 (Hyatt et al. (2010)) with the setting of “-p meta” was then used to predict the open reading frames (ORFs)  
160 of the assembled contigs. ORFs from all the available datasets were filtered (>100bp), dereplicated and merged into a  
161 catalog of non-redundant genes using cd-hit-est (>95 % sequence identity) (Fu et al. (2012)). Salmon v1.10.0 (Patro et al.  
162 (2017)) with the “- meta” option was employed to map clean reads of each dataset to the catalog of non-redundant genes  
163 and generate the GPM (genes per million reads) abundance. Eggnog mapper v2.1.12 (Cantalapiedra et al. (2021)) was then  
164 performed to assign KEGG Orthology (KO) and identify specific functional annotation for the catalog of non-redundant  
165 genes. The marker genes, *nifDK* (K02586, K02591 nitrogenase molybdenum-iron protein alpha/beta chain) and *nifH*  
166 (K02588, nitrogenase iron protein), were used for the evaluation of microbial potential of  $\text{N}_2$  fixation. *RbcL* (K01601,  
167 ribulose-bisphosphate carboxylase large chain) and *psbA* (K02703, photosystem II P680 reaction center D1 protein) were  
168 selected to evaluate the microbial potential of carbon fixation and photosynthesis, respectively. The molecular datasets  
169 have been deposited with the accession number: Bioproject PRJNA1133027.  
170

### 171 3 Results and discussion

172

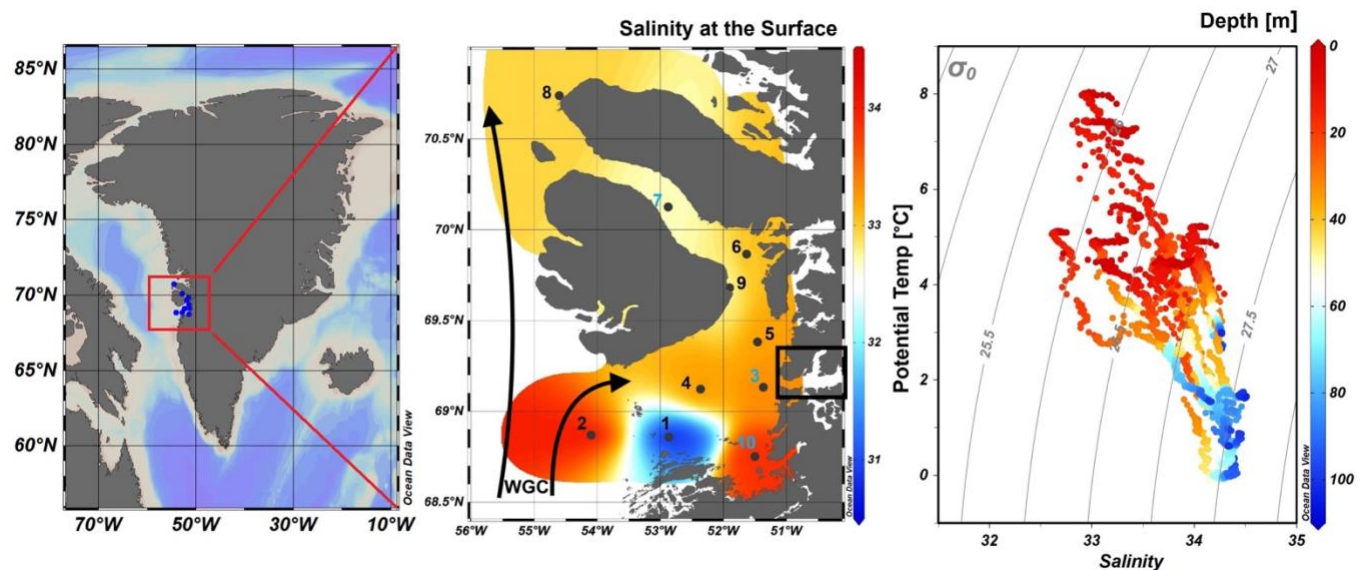
173 

### 3.1 Hydrographic conditions in Qeqertarsuaq (Disco Bay) and Sullorsuaq (Vaigat) Strait

174

175 Disko Bay (Qeqertarsuaq) is located along the west coast of Greenland (Kalaallit Nunaat) at approximately 69 °N (Figure 1), and is strongly influenced by the West Greenland Current (WGC) which is associated with the broader Baffin Bay Polar 176 Waters (BBPW) (Mortensen et al., 2022; Hansen et al., 2012). The WGC does not only significantly shape the hydrographic 177 conditions within the bay but also plays an important role in the larger context of Greenland Ice Sheet melting (Mortensen 178 et al. (2022)). Central to the hydrographic system of the Qeqertarsuaq area is the Jakobshavn Isbræ, which is the most 179 productive glacier in the northern hemisphere and believed to drain about 7 % of the Greenland Ice Sheet and thus 180 contributes substantially to the water influx into the Qeqertarsuaq (Holland et al. (2008)). A predicted increased inflow of 181 warm subsurface water, originating from North Atlantic waters, has been suggested to further affect the melting of the 182 Jakobshavn Isbræ and thus adds another layer of complexity to this dynamic system (Holland et al., 2008; Hansen et al., 183 2012).

184 The hydrographic conditions in Qeqertarsuaq have a significant influence on biological processes, nutrient availability, and the 185



186

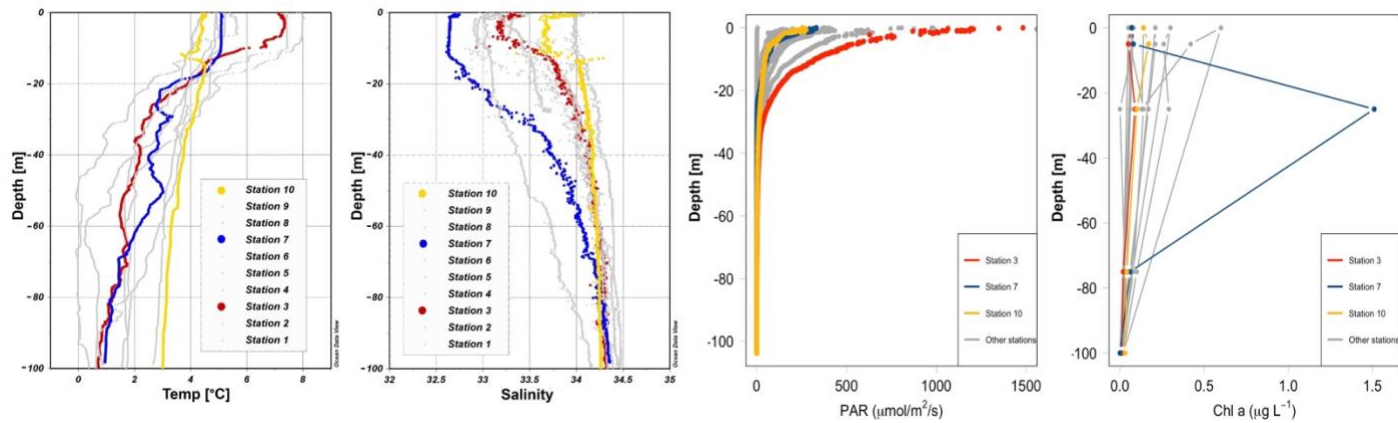
187 **Figure 1.** Map of Greenland (Kalaallit Nunaat) with indication of study area (red box), on the left. Interpolated distribution of Sea 188 Surface Salinity (SSS) values with corresponding isosurface lines and indication of 10 sampled stations (normal stations in black, 189 incubation stations in blue), black arrows indicate the West Greenland Current (WGC) and the black box indicate the location of the 190 Jakobshavn Isbræ, in the middle. Scatterplot of the potential temperature and salinity for all station data. The plot is used for the 191 identification of the main water masses within the study area. Isopycnals ( $\text{kg m}^{-3}$ ) are depicted in grey lines, on the right. Figures were 192 created in Ocean Data View (ODV) (Schlitzer (2022)).

193

194 broader marine ecosystem (Munk et al., 2015; Hendry et al., 2019; Schiøtt, 2023).

195 During our survey, we found very heterogenous hydrographic conditions at the different stations across Qeqertarsuaq (Fig. 1  
196 & Fig. 2). The three selected stations for N<sub>2</sub> fixation analysis (stations 3, 7, and 10) were strategically chosen to capture the  
197 spatial

198 variability of the area. Surface salinity and temperature measurements at these stations indicate the influence of freshwater  
199 input. The surface temperature exhibit a range of 4.5 to 8 °C, while surface salinity varies between 31 and 34, as illustrated  
200 in Fig. 1. The profiles sampled during our survey extend to a maximum depth of 100 m. Comparison of temperature/salinity  
201 (T/S) plots with recent studies suggests the presence of previously described water masses, including Warm Fjord Water  
202 (WFjW) and Cold Fjord Water (CFjW) with an overlaying surface glacial meltwater runoff. Those water masses are defined  
203 with a density range of  $27.20 \leq \sigma_0 \leq 27.31$  but different temperature profiles. Thus water masses can be differentiated by  
204 their temperature within the same density range (Gladish et al. (2015)). Other water masses like upper subpolar mode water  
205 (uSPMW), deep subpolar mode water (dSPMW) and Baffin Bay polar Water (BBPW) which has been identified in the  
206 Disko Bay (Qeqertarsuaq) before, cannot be identified from this data and may be present in deeper layers (Mortensen et  
207 al., 2022; Sherwood et al., 2021; Myers and Ribergaard, 2013; Rysgaard et al., 2020). The temperature and salinity profiles  
208 across the 10



209  
210  
211  
212 **Figure 2.** Profiles of temperature (°C), salinity, photosynthetically active radiation (PAR) ( $\mu\text{mol}/\text{m}^2/\text{s}$ ) and Chl *a* ( $\text{mg m}^{-3}$ ) across stations  
213 1 to 10 with depth (m). Stations 3, 7, and 10 are highlighted in red, blue, and yellow, respectively, to emphasize incubation stations.  
214 Figures were created in Ocean Data View and R-Studio (Schlitzer (2022)).

215 stations in the study area show distinct stratification and variability, which is represented through the three incubation  
216 stations (highlighted stations 3, 7, and 10 in Fig. 2). They display varying degrees of stratification and mixing, with notable  
217 differences in the salinity and temperature profiles. Station 3 and station 7 exhibit clear stratification in both temperature  
218 and salinity marked by the presence of thermoclines and haloclines. These features suggest significant freshwater input  
219 influenced by local weather conditions and climate dynamics, like surface heat absorption. In contrast, Station 10 exhibits a  
220 narrower range of temperature and salinity values throughout the water column compared to Stations 3 and 7, indicating  
221

222 more well-mixed conditions. This uniformity is likely influenced by the regional circulation pattern and partial upwelling  
223 (Hansen et al., 2012; Krawczyk et al., 2022). The distinct characteristics observed at station 10, as illustrated in the surface  
224 plot (Fig. 1), show an elevated salinity and colder temperatures compared

225 to the other stations. This feature suggests upwelling of deeper waters along the shallower shelf, likely facilitated by the  
226 local seafloor topography. Specifically, the seafloor shallowing off the coast of Station 10 may act as a barrier, disrupting  
227 typical circulation and forcing deeper, saltier, and colder waters to the surface. This pattern aligns with previous studies that  
228 describe similar mechanisms in the region (Krawczyk et al. (2022)). Their description of the bathymetry in Qeqertarsuaq,  
229 featuring depths ranging from ca. 50 to 900 m, suggests its impact on turbulent circulation patterns, leading to the mixing  
230 of different water masses. Evident variability in oceanographic conditions that can be observed throughout the study area  
231 occurs particularly along characteristic topographical features like steep slopes, canyons, and shallower areas. The summer  
232 melting of sea ice and glaciers introduces freshwater influxes that create distinct vertical and horizontal gradients in salinity  
233 and temperature in the Qeqertarsuaq area Hansen et al. (2012). Additionally, the accelerated melting of the Jakobshavn  
234 Isbraæ, influenced by the warmer inflow from the West Greenland Intermediate Current (WGIC), further alters the  
235 hydrographic conditions. Recent observations indicate significant warming and shoaling of the WGIC, potentially enabling  
236 it to overcome the sill separating the Ilulissat Fjord from the Qeqertarsuaq area (Hansen et al., 2012; Holland et al., 2008;  
237 Myers and Ribergaard, 2013). This shift intensifies glacier melting, driving substantial changes in the local ecological  
238 dynamics (Ardyna et al., 2014; Arrigo et al., 2008; Bhatia et al., 2013).

### 239 **3.2 N<sub>2</sub> Fixation Rate Variability and Associated Environmental Conditions**

240  
241 We quantified N<sub>2</sub> fixation rates within the waters of Qeqertarsuaq, spanning from the surface to a depth of 50 m (Table 1).  
242 The rates ranged from 0.16 to 2.71 nmol N L<sup>-1</sup> d<sup>-1</sup> with all rates surpassing the minimum quantifiably rate (Appendix  
243 Table 1). Our findings represent rates at the upper range of those observed in the Arctic Ocean. Previous measurements in  
244 the region have been limited, with only one study in Baffin Bay by Blais et al. (2012), reporting rates of 0.02 nmol N L<sup>-1</sup> d<sup>-1</sup>,  
245 which are 1-2 orders of magnitude lower than our observations. Moreover, Sipler et al. (2017), reported rated in the coastal  
246 Chukchi Sea, with average values of 7.7 nmol N L<sup>-1</sup> d<sup>-1</sup>. These values currently represent some of the highest rates measured  
247 in Arctic shelf environments. Compared to these, our highest measured rate (2.71 nmol N L<sup>-1</sup> d<sup>-1</sup>) is lower, but still  
248 important, particularly considering the more Atlantic-influenced location of our study site. Sipler et al. (2017) also noted  
249 that a significant fraction of diazotrophs were <3 µm in size, suggesting that small unicellular diazotrophs play a dominant  
250 role in Arctic nitrogen fixation. Altogether, our data contribute to the growing evidence that N<sub>2</sub> fixation is a widespread  
251 and potentially significant nitrogen source across various Arctic regions. Simultaneous primary production rate  
252 measurements ranged from 0.07 to 3.79 µmol N L<sup>-1</sup> d<sup>-1</sup>, with the highest rates observed at station 7 and generally higher  
253 values in the surface layers. Employing Redfield stoichiometry, the measured N<sub>2</sub> fixation rates accounted for 0.47 to 2.6 %  
254 (averaging 1.57 %) of primary production at our stations. The modest contribution to primary production suggests that N<sub>2</sub>  
255 fixation does not exert a substantial influence on the productivity of these waters during the time of the sampling. Rather,

256 our N<sub>2</sub> fixation rates suggest primary production to depend mostly on additional nitrogen sources including regenerated,  
257 meltwater or land-based sources.

258 While the N:P ratio is commonly used to assess nutrient limitations relative to Redfield stoichiometry, most DIN and DIP  
259 measurements in our study were below detection limit (BDL), preventing a reliable calculation for this ratio. As such, we  
260 refrain from drawing conclusions based on N:P stoichiometry. Nevertheless, previous studies by Jensen et al. (1999) and  
261 Tremblay and Gagnon (2009), have identified nitrogen limitation in this region. Such biogeochemical conditions, when  
262 present, would be expected to generate a niche for N<sub>2</sub> fixing organisms (Sohm et al. (2011)). While N<sub>2</sub> fixation did not  
263 chiefly sustain primary production during our sampling campaign, we hypothesize that N<sub>2</sub> fixation has the potential to play  
264 a role in bloom dynamics under certain conditions. As nitrogen availability decreases

265 during a bloom, it may provide a niche for N<sub>2</sub> fixation, potentially helping to extend the productive period of the bloom  
266 period (Reeder et al. (2021)). Satellite data indicates that a fall bloom began in early August, following the annual spring  
267 bloom, as described by Ardyna et al. (2014). This double bloom situation may be driven by increased melting and the  
268 subsequent input of bioavailable nutrients and iron (Fe) from meltwater runoff (Arrigo et al., 2017; Hopwood et al., 2016;  
269 Bhatia et al., 2013). The meltwater from the Greenland Ice Sheet is a significant source of Fe (Bhatia et al., 2013; Hawkings  
270 et al., 2015, 2014), which is a limiting factor especially for diazotrophs (Sohm et al. (2011)). Consequently, it is plausible  
271 that Fe and nutrients from the Isbræ glacier create favorable conditions for both bloom development and diazotroph activity  
272 in Qeqertarsuaq. However, we emphasize that confirming a causal link between N<sub>2</sub> fixation and secondary bloom  
273 development requires further evidence, such as time-series data on nutrient concentrations, diazotroph abundance, and  
274 bloom dynamics.

275  
276 **Table 1.** N<sub>2</sub> fixation (nmol N L<sup>-1</sup> d<sup>-1</sup>), standard deviation (SD), primary productivity (PP;  $\mu\text{mol C L}^{-1} \text{d}^{-1}$ ), SD, percentage of estimated  
277 new primary productivity (% New PP) sustained by N<sub>2</sub> fixation, dissolved inorganic nitrogen compounds (NO<sub>x</sub>), phosphorus (PO<sub>4</sub>), and  
278 the molar nitrogen-to-phosphorus ratio (N:P) at stations 3, 7, and 10. BDL= Below detection limit.  
279

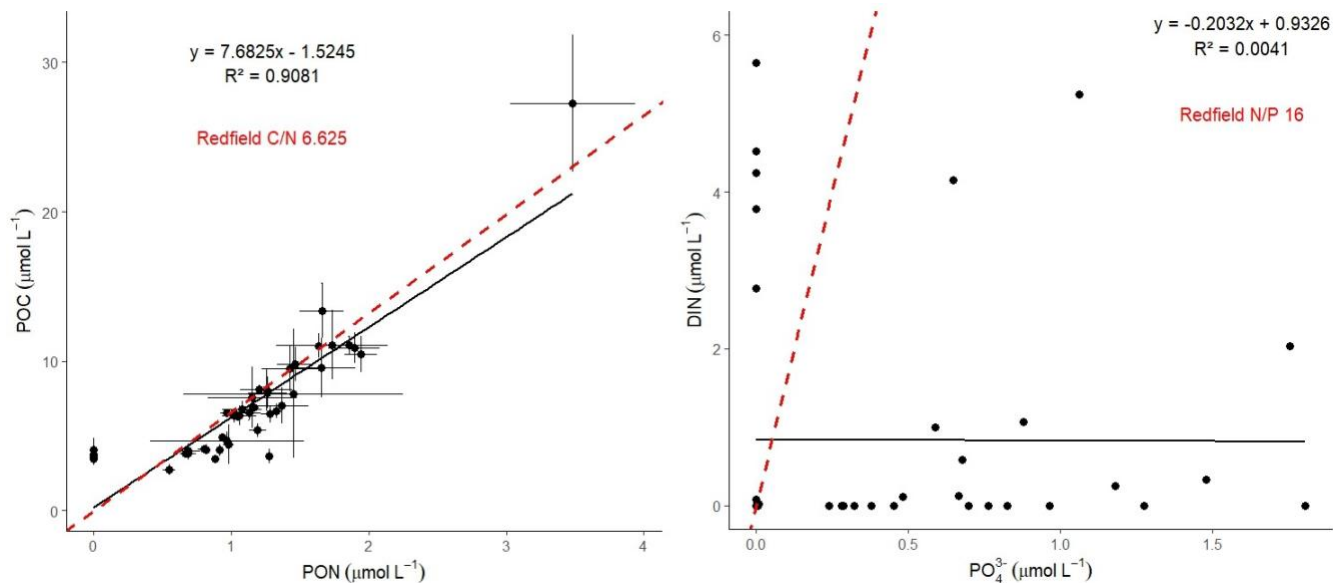
Station (no.)	Depth (m)	N <sub>2</sub> fixation (nmol N L <sup>-1</sup> d <sup>-1</sup> )	SD ( $\pm$ )	Primary Productivity ( $\mu\text{mol C L}^{-1} \text{d}^{-1}$ )	SD ( $\pm$ )	% New PP (%)	NO <sub>x</sub> ( $\mu\text{mol L}^{-1} \text{d}^{-1}$ )	PO <sub>4</sub> ( $\mu\text{mol L}^{-1} \text{d}^{-1}$ )
3	0	1.20	0.21	0.466	0.08	1.71	BDL	BDL
3	25	1.88	0.11	0.588	0.04	2.11	BDL	0.70
3	50	0.29	0.01	0.209	0.00	0.91	0.33	1.48
7	0	2.49	0.44	0.63	0.20	2.60	BDL	BDL
7	25	2.71	0.22	3.79	2.45	0.47	BDL	0.45
7	50	0.53	0.24	0.33	0.36	1.08	BDL	0.97
10	0	1.48	0.12	0.74	0.15	1.33	BDL	BDL

10	25	0.31	0.01	0.29	0.07	0.73	BDL	BDL
10	50	0.16	0	0.07	0.07	1.40	BDL	BDL

280 A near-Redfield stoichiometry in POC:PON suggests that the particulate organic matter (POM) likely originates from an  
 281 ongoing phytoplankton bloom, as phytoplankton generally assimilate carbon and nitrogen in relatively consistent  
 282 proportions during active growth (Redfield 1934). However this assumption is based on a global average, and POM  
 283 stoichiometry can exhibit substantial latitudinal variation. Deviations may also arise during particle production and  
 284 remineralization processes (Redfield 1934; Geider and La Roche 2002; Sterner and Elser 2017; Quigg et al., 2003). Recent  
 285 studies have further shown that POM composition vary widely across plankton communities, influenced by factors such as  
 286 growth rates, community composition, ad physiological status (e.g. fast- vs- slow-growing organisms), with degradation  
 287 often playing a secondary role (Tanioka et al., 2022). Additionally, terrestrial organic material—likely introduced via glacial  
 288 outflow in the study area—may also contribute to the observed POM composition (Schneider et al., 2003). Latitudinal  
 289 variability in organic matter stoichiometry has also been linked to differences in nutrient supply and phosphorus stress  
 290 (Fagan et al., 2024; Tanioka et al., 2022). Consequently, the near-Redfield stoichiometry observed here cannot be clearly  
 291 attributed to freshly produced organic material. Nevertheless, satellite-derived surface chlorophyll *a* concentration and  
 292 associated primary production support the interpretation that recently produced organic matter does contribute, at least in  
 293 part, to the sinking POM captured in our samples. Since inorganic nitrogen species (e.g., NOx) were below detection limits,  
 294 direct calculation or interpretation of the N:P ratio in the dissolved nutrient pool was not possible and has been avoided. The  
 295 absence of available nitrogen may nonetheless reflect nitrogen depletion, potentially creating ecological niches for  
 296 diazotrophs and nitrogen-fixing organisms. Such conditions may promote shifts in microbial community structure, as  
 297 observed by Laso-Perez et al. (2024). Laso Perez et al. (2024) documented changes in microbial community composition  
 298 during an Arctic bloom, focusing on nitrogen cycling. They observed a shift from chemolithotrophic to heterotrophic  
 299 organisms throughout the summer bloom and noted increased activity to compete for various nitrogen sources. However, no  
 300 *nifH* gene copies, indicative of nitrogen-fixing organisms, were found in their dataset based on metagenome-assembled  
 301 genomes (MAGs). This is not unexpected due to the classically low abundance of diazotrophs in marine microbial  
 302 communities which has often been described (Turk-Kubo et al., 2015; Farnelid et al., 2019). Given the high productivity  
 303 and metabolic activity observed in Qeqertarsuaq during a similar bloom period, the detected diazotrophs (Section 3.3) may  
 304 play a more significant role than previously thought. Across the 10 stations there is considerable variability in POC and PON  
 305 concentrations (Fig. 3). PON concentrations range from 0.0  $\mu\text{mol N L}^{-1}$  to 3.48  $\mu\text{mol N L}^{-1}$  (n=124), while POC  
 306 concentrations range from 2.7  $\mu\text{mol C L}^{-1}$  to 27.2  $\mu\text{mol C L}^{-1}$  (n=144). The highest concentrations for both PON and POC  
 307 were observed at station 7 at a depth of 25 m and coincide with the highest reported N<sub>2</sub> fixation rate (Figure Appendix A2  
 308 & A3). Generally, POC and PON concentrations decrease with depth, peaking at the deep chl *a* maximum (DCM), identified  
 309 between 15 to 30 m across all stations. The DCM was identified based on measured chl *a* concentrations and previous  
 310 descriptions in the region (Fox and Walker, 2022; Jensen et al., 1999). The variability in chl *a* concentrations indicates

312 differences in phytoplankton abundance among the stations, with concentrations ranging between 0 to  $0.42 \text{ mg m}^{-3}$ . Excluding  
 313 station 7, which exhibited the highest chl *a* concentration at the DCM ( $1.51 \text{ mg m}^{-3}$ ). While Tang et al. (2019) found that  $\text{N}_2$   
 314 fixation measurements strongly correlated to satellite estimates of chl *a* concentrations, our results did not show a statistically  
 315 significant correlation between nitrogen fixation rates and chl *a* concentrations overall (Figures A2 & A3). However, as  
 316 noted, Station 7 at 25 m represents a unique case. The elevated concentration of chl *a* at this station likely resulted from a  
 317 local phytoplankton bloom induced by meltwater outflow from the Isbræ glacier and sea ice melting, which may help explain  
 318 the observed nitrogen fixation rates (Arrigo et al., 2017; Wang et al., 2014). This study's findings are in agreement with  
 319 prior reports of analogous blooms occurring in the region (Fox and Walker, 2022; Jensen et al., 1999).

320



321  
 322 **Figure 3.** The POC/PON and DIN/DIP ratios at all 10 stations. The red line represents the Redfield ratios of POC/PON (106:16) and  
 323 DIN/DIP (16:1).

324

325

### 326 3.3 Potential Contribution of UCYN-A to Nitrogen Fixation During a Diatom Bloom: Insights and Uncertainties

327  
 328 In our metagenomic analysis, we filtered the *nifH*, *nifD*, *nifK* genes, which code for the nitrogenase enzyme responsible  
 329 for catalyzing  $\text{N}_2$  fixation. We could identify sequences related to UCYN-A, which dominated the sequence pool of  
 330 diazotrophs, particularly in the upper water masses (0 to 5 m) (Fig. 4). UCYN-A, a unicellular cyanobacterial symbiont, has  
 331 a cosmopolitan distribution and is thought to substantially contribute to global  $\text{N}_2$  fixation, as documented by (Martínez-  
 332 Pérez et al., 2016; Tang et al., 2019). This conclusion is based on our metagenomic analysis, in which we set a sequence  
 333 identity threshold of 95% for both *nif* and photosystem genes. Notably, we only recovered sequences related to UCYN-A

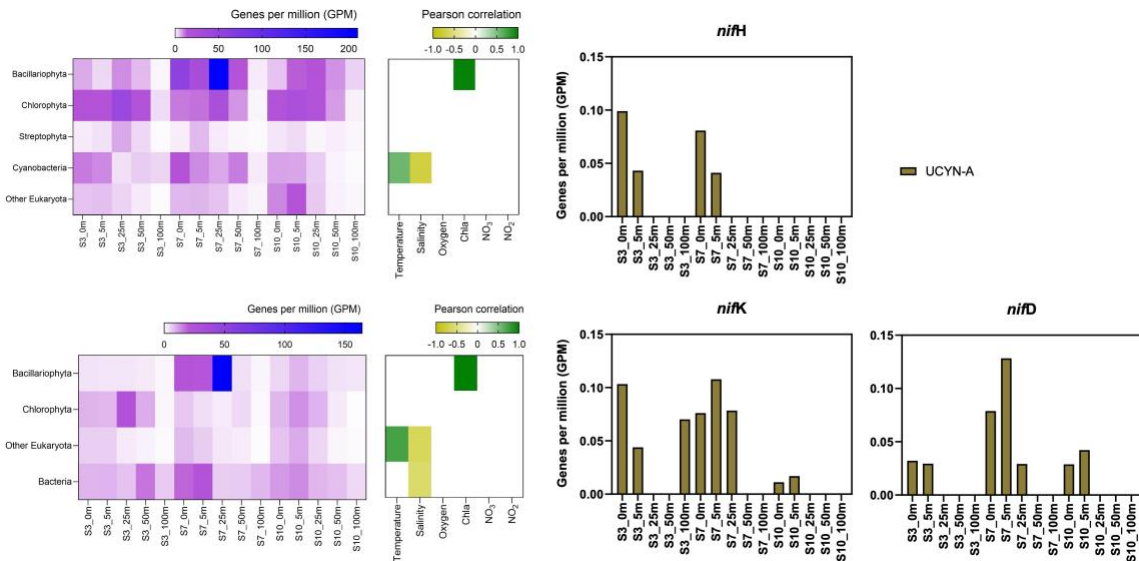
334 within our *nif* sequence pool, suggesting its predominance among detected diazotrophs. However, metagenomic  
335 approaches may underestimate overall diazotroph diversity, and we cannot fully exclude the presence of other, less  
336 abundant diazotrophs that may have been missed using this method. While UCYN-A was primarily detected in surface  
337 waters, we also observed relatively high *nifK* values at S3\_100m, an unusual finding given that UCYN-A is typically  
338 constrained to the euphotic zone. Previous studies have predominantly reported UCYN-A in surface waters; for instance  
339 Harding et al. (2018) and Shiozaki et al. (2017) detected UCYN-A exclusively in the upper layers of the Arctic Ocean.  
340 Additionally, Shiozaki et al. (2020) found UCYN-A2 at depths extending to the 0.1% light level but not below 66 m in the  
341 Chukchi Sea. The detection of UCYN-A at 100 m in our study suggests that alternative mechanisms, such as particle  
342 association, vertical transport, or local environmental conditions, may facilitate its presence at depth. Interestingly, despite  
343 very low *nifH* copy numbers being reported in nearby Baffin Bay by Robicheau et al. (2023), UCYN-A dominated the  
344 metagenomic *nifH* community in our study, further underscoring this organism's presence in Arctic surface coastal areas  
345 under certain environmental conditions. This warrants further investigation into the environmental drivers and potential  
346 processes enabling its occurrence in Arctic waters.

347 Due to the lack of genes such as those encoding Photosystem II and Rubisco, UCYN-A plays a significant role within the  
348 host cell and participates in fundamental cellular processes. Consequently, it has evolved to become a closely integrated  
349 component of the host cell. Very recent findings demonstrate that UCYN-A imports proteins encoded by the host genome  
350 and has been described as an early form of N<sub>2</sub> fixing organelle termed a "Nitroplast" (Coale et al. (2024)).

351 Previous investigations document that they are critical for primary production, supplying up to 85% of the fixed nitrogen to  
352 their haptophyte host (Martínez-Pérez et al. (2016)). In addition to its high contribution to primary production, studies have  
353 shown that UCYN-A in high latitude waters fix similar amounts of N<sub>2</sub> per cell as in the tropical Atlantic Ocean, even in  
354 nitrogen- replete waters (Harding et al., 2018; Shiozaki et al., 2020; Martínez-Pérez et al., 2016; Krupke et al., 2015; Mills  
355 et al., 2020). However, estimating their contribution to N<sub>2</sub> fixation in our study is challenging, particularly since we detected  
356 cyanobacteria only at the surface but observe significant N<sub>2</sub> fixation rates below 5 m. The diazotrophic community is often  
357 underrepresented in metagenomic datasets due to the low abundance of nitrogenase gene copies, implying our data does  
358 not present a complete picture. We suspect a more diverse diazotrophic community exists, with UCYN-A being a significant  
359 contributor to N<sub>2</sub> fixation in Arctic waters. However, the exact proportion of its contribution requires further investigation.  
360 The contribution of N<sub>2</sub> fixation to carbon fixation (as percent of PP) is relatively low, at the time of our study. We identified  
361 genes such as *rbcL*, which encodes Rubisco, a key enzyme in the carbon fixation pathway and *psbA*, a gene encoding  
362 Photosystem II, involved in light-driven electron transfer in photosynthesis, in our metagenomic dataset. The gene *rbcL* (for  
363 the carbon fixation pathway) and the gene *psbA* (for primary producers) were used to track the community of photosynthetic  
364 primary producers in our metagenomic dataset. At station 7, elevated carbon fixation rates are correlated with high diatom  
365 (*Bacillariophyta*) abundance and increased chl *a* concentration (Fig. 4), suggesting the onset of a bloom, which is also  
366 observable via satellite images (Appendix A1). We hypothesize that meltwater, carrying elevated nutrient and trace metal  
367 concentrations, was rapidly transported away from the glacier through the Vaigat Strait by strong winds, leading to increased

productivity, as previously described by Fox and Walker (2022) & Jensen et al. (1999). The elevated diatom abundance and primary production rates at station 7 coincide with the highest N<sub>2</sub> fixation rates, which could point toward a possible diatom-diazotroph symbiosis (Foster et al., 2022, 2011; Schvarcz et al., 2022). However, we did not detect a clear diazotrophic signal directly associated with the diatoms in our metagenomic dataset, which might be due to generally underrepresentation of diazotrophs in metagenomes due to low abundance or low sequencing coverage. To investigate this further, we examined the taxonomic composition of *Bacillariophyta* at higher resolution. Among the various abundant diatom genera, *Rhizosolenia* and *Chaetoceros* have been identified as symbiosis with diazotrophs (Grosse, et al., 2010; Foster, et al., 2010), representing less than 6% or 15% of *Bacillariophyta*, based on *rbcL* or *psbA*, respectively (Figure Appendix A4). Although we underestimate diazotrophs to an extent, the presence of certain diatom-diazotroph symbiosis could help explain the high nitrogen fixation rates in the diatom bloom to a certain degree. Compilation of *nif* sequences identified from this study as well as homologous from their NCBI top hit were added in Table S1. However, we cannot tell if the diazotrophs belong to UCYN-A1 or UCYN-A2, or UCYN-A3. Based on the Pierella Karlusich et al. (2021), they generated clonal *nifH* sequences from Tara Oceans, which the length of *nifH* sequences is much shorter than the two *nifH* sequences we generated in our study. Also, the available UCYN-A2 or UCYN-A3 *nifH* sequences from NCBI were shorter than the two *nifH* sequences we generated. Therefore, it would be not accurate to assign the *nifH* sequences to either group under UCYN-A. Furthermore, not much information is available regarding the different groups of UCYN-A using marker genes of *nifD* and *nifK*.

385



386  
387

388  
389 **Figure 4.** Upper left image: *psbA* with correlation plot. Lower left image: *rbcL* with correlation plot. Right image: *nifH*, *nifD*, *nifK* genes per million reads in the metagenomic datasets. All figures display molecular data from metagenomic dataset for all sampled depth of station 3,7,10

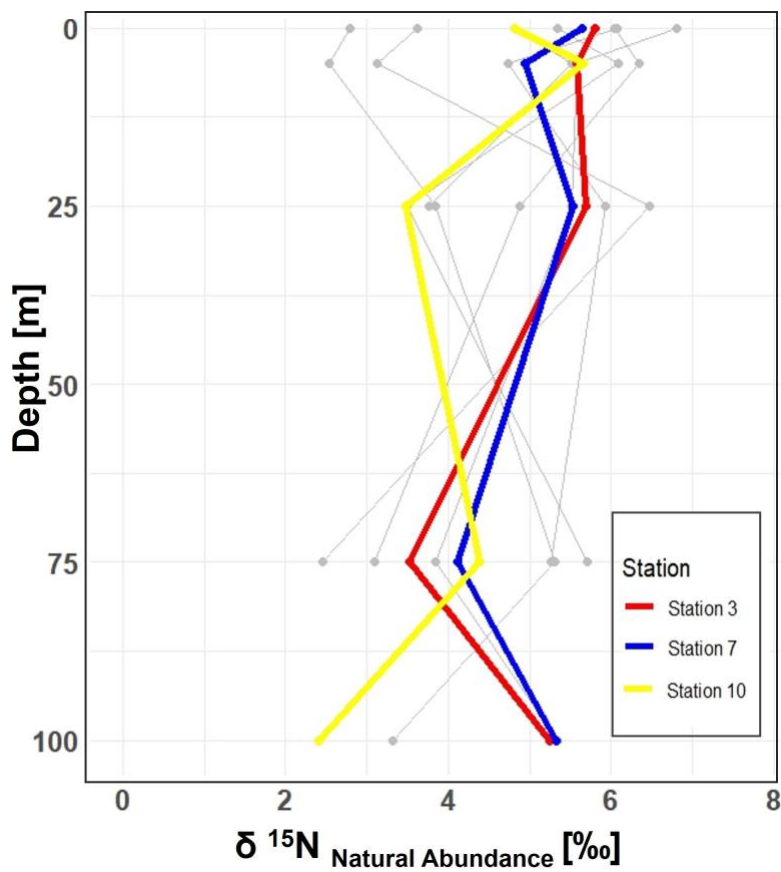
392 There is evidence that UCYN-A have a higher Fe demand, with input through meltwater or river runoff potentially being  
393 advantageous to those organisms (Shiozaki et al., 2017, 2018; Cheung et al., 2022). Consequently, UCYN-A might play a  
394 more critical role in the future with increased Fe-rich meltwater runoff. UCYN-A can potentially fuel primary productivity  
395 by supplying nitrogen, especially with increased melting, nutrient inputs, and more light availability due to rising  
396 temperatures as- sociated with climate change. This predicted enhancement of primary productivity may contribute to the  
397 biological drawdown of CO<sub>2</sub>, acting as a negative feedback mechanism. These projections are based on studies forecasting  
398 increased temperatures, melting, and resulting biogeochemical changes leading to higher primary productivity. However  
399 large uncertainties make pre- dictions very difficult and should be handled with care. Thus, we can only hypothesize that  
400 UCYN-A might be coupled to these dynamics by providing essential nitrogen.  
401

#### 402 3.4 $\delta^{15}\text{N}$ Signatures in particulate organic nitrogen

403 Stable isotopic composition, expressed using the  $\delta^{15}\text{N}$  notation, serve as indicators for understanding nitrogen dynamics  
404 because different biogeochemical processes fractionate nitrogen isotopes in distinct ways (Montoya (2008)). However, it  
405 is important to keep in mind that the final isotopic signal is a combination of all processes and an accurate distinction  
406 between processes cannot be made. N<sub>2</sub> fixation tends to enrich nitrogenous compounds with lighter isotopes, producing  
407 OM with isotopic values ranging approximately from -2 to +2 ‰ (Dähnke and Thamdrup (2013)). Upon complete  
408 remineralization and oxidation, organic matter contributes to a reduction in the average  $\delta$ -values in the open ocean  
409 (e.g. Montoya et al. (2002);

411 Emeis et al. (2010)). Whereas processes like denitrification and anammox preferentially remove lighter isotopes, leading  
412 to enrichment in heavier isotopes and delta values up to -25 ‰.

413



414

415

416 **Figure 5.** Vertical profiles of  $\delta^{15}\text{N}$  natural abundance signatures in PON across 10 stations in the study area. Incubation stations 3, 7, and  
 417 10 are highlighted in red, blue, and yellow, respectively. The figure shows variations in  $\delta^{15}\text{N}$  signatures with depth at each station,  
 418 providing insight into nitrogen cycling in the study area.

419

420 In our study, the  $\delta^{15}\text{N}$  values of PON from all 10 stations, range between 2.45 ‰ and 8.30 ‰ within the 0 to 100 m depth  
 421 range. While  $\text{N}_2$  fixation typically produces OM ranging from -2 ‰ to 0.5 ‰, this signal can be masked by processes such as  
 422 remineralization, mixing with nitrate from deeper waters or other biological transformations (Emeis et al. (2010); Sigman  
 423 et al. (2009)). The composition of OM in the surface ocean is influenced by the nitrogen substrate and the fractionation  
 424 factor during assimilation. When nitrate is depleted in the surface ocean, the isotopic signature of OM produced during  
 425 photosynthesis will mirror that of the nitrogen source. Nitrate, the primary form of dissolved nitrogen in the open ocean,  
 426 typically exhibits an average stable isotope value of around

427 5 ‰. No fractionation occurs during photosynthesis because the nitrogen source is entirely taken up in the surface waters  
 428 (Sigman et al. (2009)). This matches conditions observed in Qeqertarsuaq, suggesting that subsurface nitrate is a dominant

429 nitrogen source (Fox and Walker (2022)).

430 In the eastern Baffin Bay waters, Atlantic water masses serve as an important source of nitrate to surface waters with  $\delta^{15}\text{N}$   
431 values around 5‰ (Sherwood et al. (2021)). This is consistent with our observed PON values and supports the view that  
432 primary productivity in the region is largely fueled by nitrate input from deeper Atlantic waters, particularly during early  
433 bloom stages (Fox and Walker, 2022; Knies, 2022). The mechanisms through which subsurface nitrate reaches the euphotic  
434 layer are not well understood. However, potential pathways include vertical migration of phytoplankton and physical  
435 mixing. Subsequently, nitrogen undergoes rapid recycling and remineralization processes to meet the system's nitrogen  
436 demands (Jensen et al. (1999)). Taken together, the  $\delta^{15}\text{N}$  signatures observed in this study are best interpreted as indicative  
437 of a system influenced by multiple nitrogen sources and biogeochemical processes, where nitrate input and remineralization  
438 appear to dominate.

#### 440 441 **4 Conclusion**

442 Our study highlights the occurrence of elevated rates of  $\text{N}_2$  fixation in Arctic coastal waters, particularly prominent at station  
443 7, where they coincide with high chl *a* values, indicative of heightened productivity. Satellite observations tracing the origin  
444 of a bloom near the Isbræ Glacier, subsequently moving through the Vaigat strait, suggest a recurring phenomenon likely  
445 triggered by increased nutrient-rich meltwater originating from the glacier. This aligns with previous reports by Jensen et  
446 al. (1999) & Fox and Walker (2022), underlining the significance of such events in driving primary productivity in the region.  
447 The contribution of  $\text{N}_2$  fixation to primary production was low (average 1.57 %) across the stations. Since the demand was  
448 high relative to the new nitrogen provided by  $\text{N}_2$  fixation, the observed primary production must be sustained by the already  
449 present or adequate amount of subsurface supply of  $\text{NO}_x$  nutrients in the seawater. This is also visible in the isotopic signature  
450 of the POM (Fox and Walker, 2022; Sherwood et al., 2021). However, the detected  $\text{N}_2$  fixation rates are likely linked to the  
451 development of the fresh secondary summer bloom, which could be sustained by high nutrient and Fe availability from  
452 melting, potentially leading the system into a nutrient-limited state. The ongoing high demand for nitrogen compounds may  
453 suggest an onset to further sustain the bloom, but it remains speculative whether Fe availability definitively contributes to  
454 this process. The occurrence of such double blooms has increased by 10 % in the Qeqertarsuaq and even 33 % in the Baffin  
455 Bay, with further projected increases moving north from Greenland (Kalaallit Nunaat) waters (Ardyna et al. (2014)). Thus,  
456 nutrient demands are likely to increase, and the role of  $\text{N}_2$  fixation can become more significant. The diazotrophic community  
457 in this study is dominated by UCYN-A in surface waters and may be linked to diatom abundance in deeper layers. This co-  
458 occurrence of diatoms and  $\text{N}_2$  fixers in the same location is probably due to the co-limitation of similar nutrients, rather than  
459 a symbiotic relationship. Thus, this highlights the significant presence of diazotrophs despite their limited representation in  
460 datasets. It also highlights the potential for further discoveries, as existing datasets likely underestimate the full extent of  
461 the diazotrophic community (Laso Perez et al., 2024);

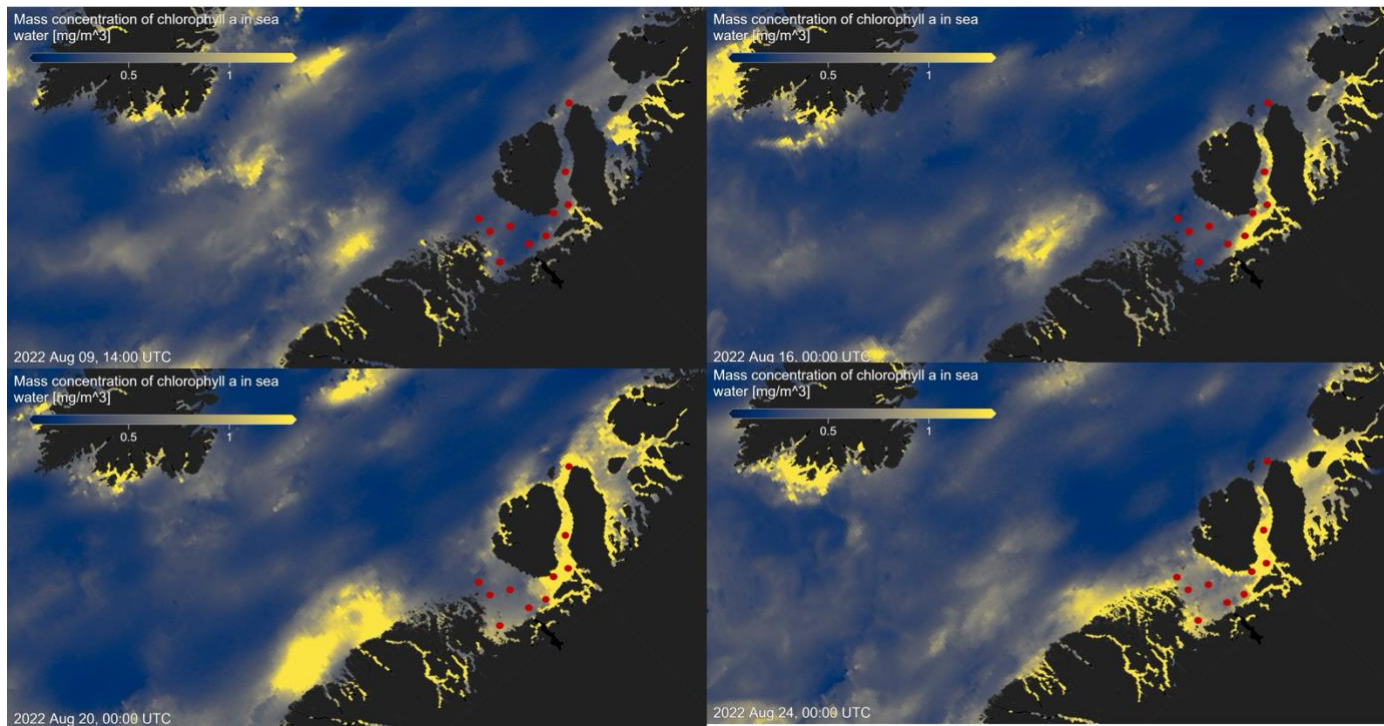
463 Shao et al., 2023; Shiozaki et al., 2017, 2023). The reported N<sub>2</sub> fixation rates in the Vaigat strait within the Arctic Ocean  
464 are notably higher than those observed in many other oceanic regions, emphasizing that N<sub>2</sub> fixation is an active and  
465 significant process in these high-latitude waters. When compared to measured rates across various ocean systems using the  
466 <sup>15</sup>N approach, the significance of these findings becomes clear. For instance, N<sub>2</sub> fixation rates are sometimes below the  
467 detection limit and often relatively low ranging from 0.8 to 4.4 nmol N L<sup>-1</sup> d<sup>-1</sup> (Löscher et al., 2020, 2016; Turk et al., 2011).  
468 In contrast, higher rates reach up to 20 nmol N L<sup>-1</sup> d<sup>-1</sup> (Rees et al. (2009)) and sometime exceptional high rates range from  
469 38 to 610 nmol N L<sup>-1</sup> d<sup>-1</sup> (Bonnet et al. (2009)). The Arctic Ocean rates are thus significant in the global context,  
470 underscoring the region's role in the global nitrogen cycle and the importance of N<sub>2</sub> fixation in supporting primary  
471 productivity in these waters.

472 These findings highlight the urgent need to understand the interplay between seasonal variations, sea-ice dynamics, and  
473 hydro- graphic conditions in Qeqertarsuaq. As climate change accelerates the melting of the Greenland Ice Sheet at  
474 Jakobshavn Isbræ, shifts in hydrodynamic patterns and hydrographic conditions in Qeqertarsuaq are anticipated. The  
475 resulting influx of warmer waters could significantly reshape the bay's hydrography, making it crucial to comprehend the  
476 coupling of climate-driven changes and oceanic processes in this vital Arctic region. Our study provides key insights into  
477 these dynamics and underscores the importance of continued investigation to predict Qeqertarsuaq's future hydrographic  
478 state. By detailing the environmental and hydrographic changes, we contribute valuable knowledge to the broader context  
479 of N<sub>2</sub> fixation in the Arctic Ocean. Given nitrogen's pivotal role in Arctic ecosystem productivity, it is essential to explore  
480 diazotrophs, quantify N<sub>2</sub> fixation, and assess their impact on ecosystem services as climate change progresses.

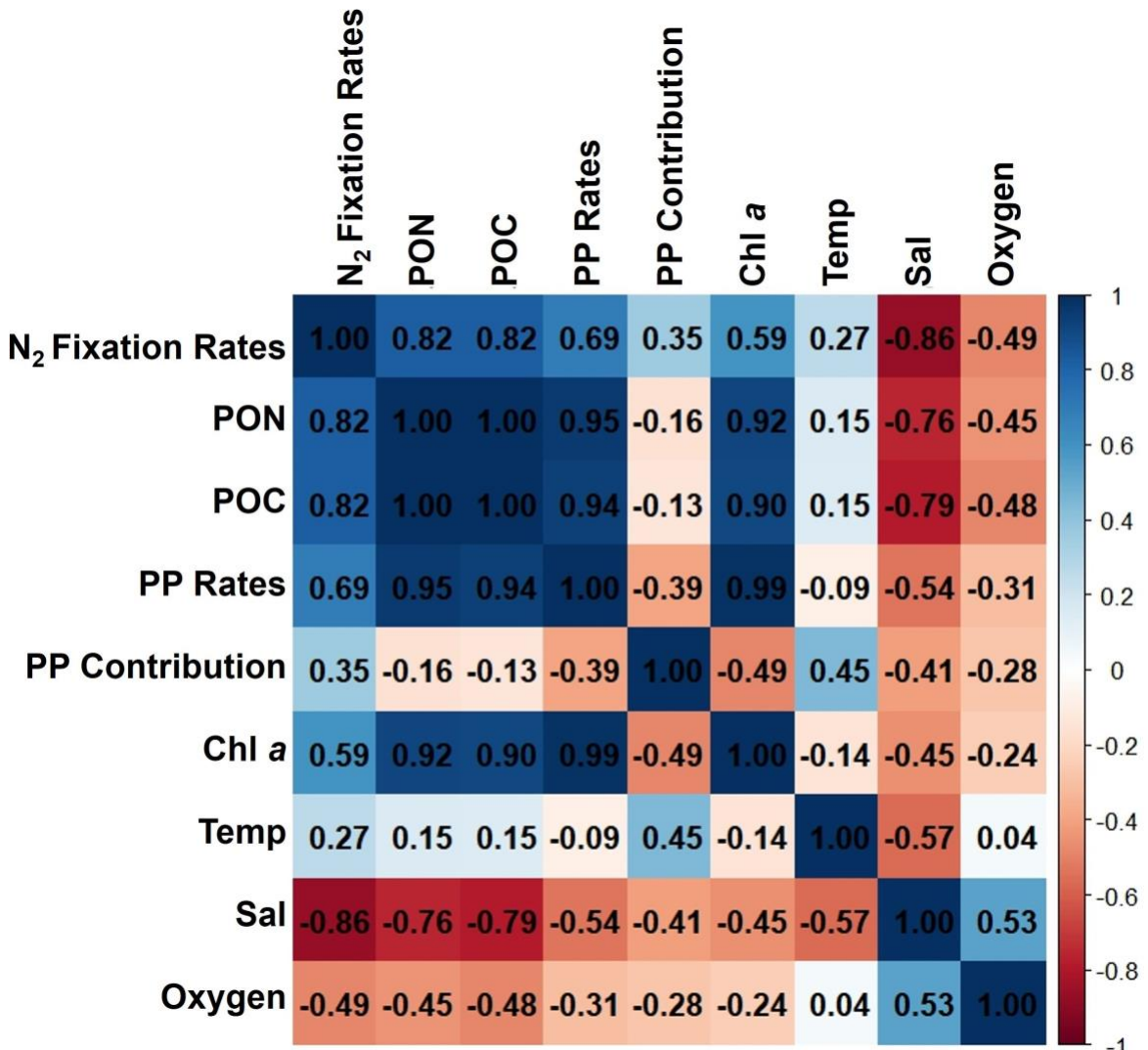
481 **Appendix A**

482

483



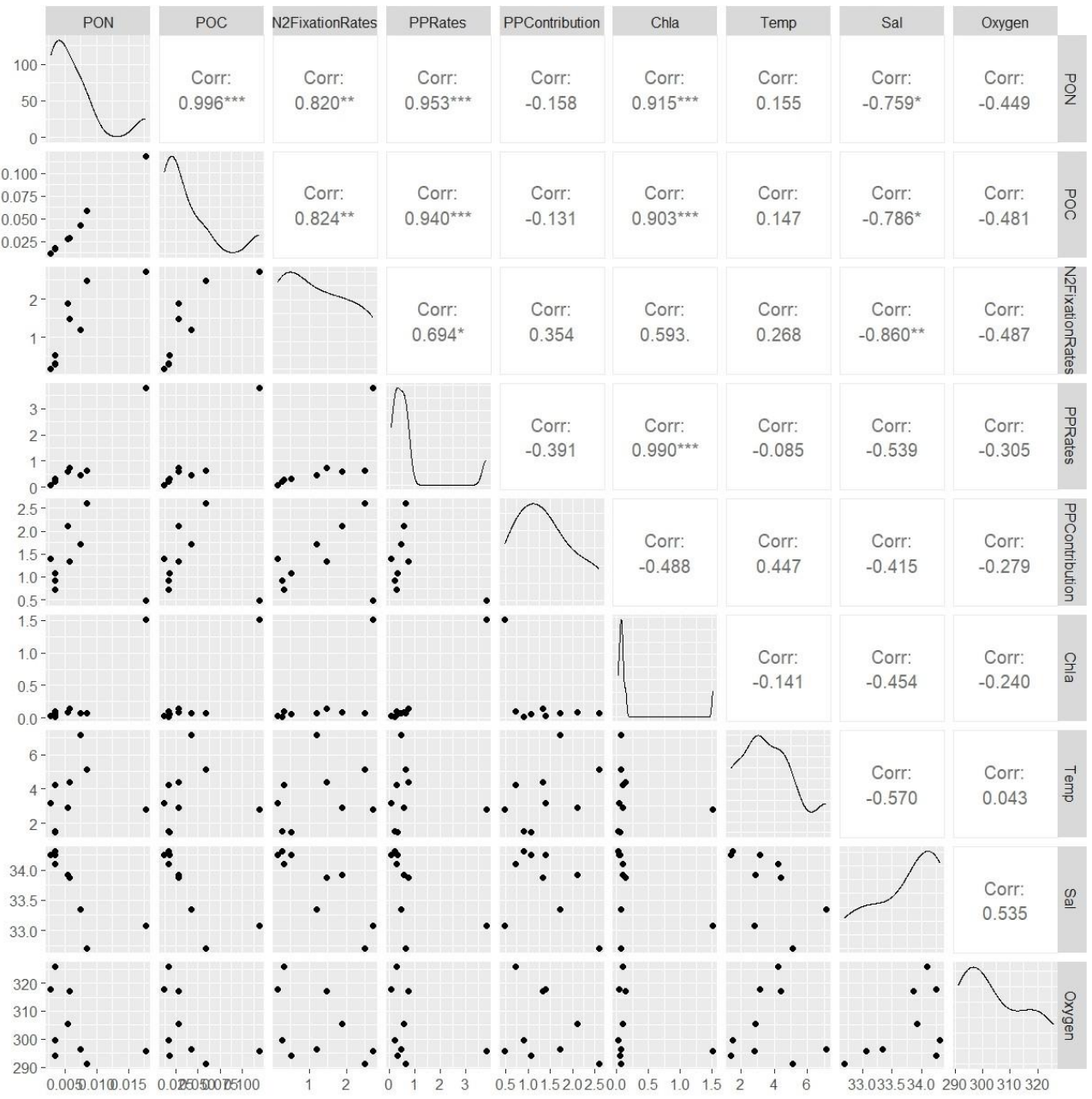
484  
485 **Figure A1.** Chlorophyll  $a$  concentration  $\text{mg m}^{-3}$  at four time points before, during, and after sea water sampling in August  
486 2022 (sampling stations indicated by red dots), obtained from MODIS-Aqua; <https://giovanni.gsfc.nasa.gov> (Aqua MODIS Global  
487 Mapped Chl  $a$  Data, version R2022.0, DOI:10.5067/AQUA/MODIS/L3M/CHL/2022), 4 km resolution, last access 03 June 2024



488

489

490 **Figure A2.** Correlation matrix of environmental and biological variables. The plot shows the correlation coefficients between the  
 491 following parameters: N<sub>2</sub> fixation rates, PON, POC, PP rates, the contribution N<sub>2</sub> fixation to PP (PP contribution), Chl a, temperature  
 492 (Temp), salinity (Sal), and Oxygen. The scale ranges from -1 to 1, where values close to 1 or -1 indicate strong positive or negative  
 493 correlations, respectively, and values near 0 indicate weak or no correlation. The color intensity represents the strength and direction of  
 494 the correlations, facilitating the identification of relationships among the variables



495

496

497

498

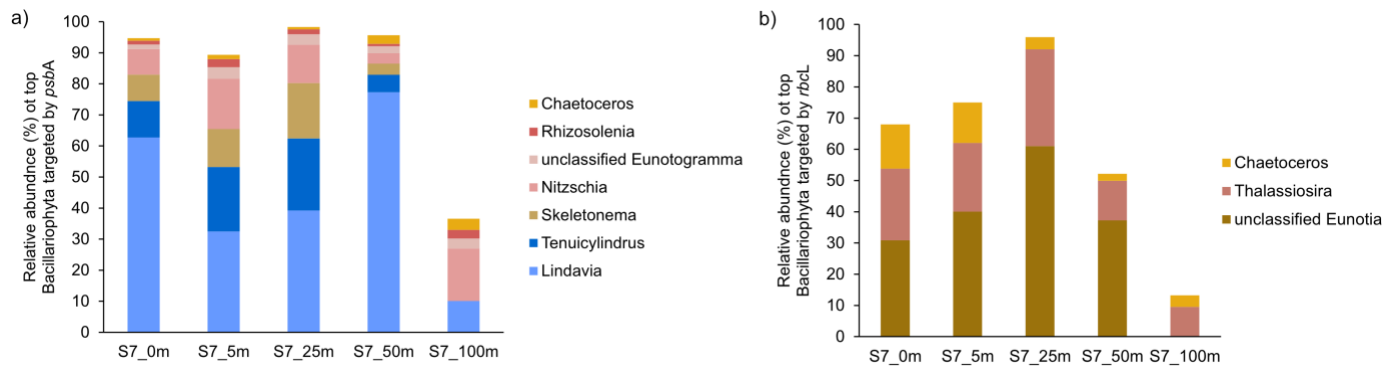
499

500

**Figure A3.** This figure displays a ggpairs plot, showing pairwise relationships and correlations between biological and environmental variables. Pearson correlation coefficients displayed in the upper triangular panel, indicating the strength and significance of linear relationships. Statistical significance levels are indicated by stars (\*), where \* indicates  $p < 0.05$ , \*\* indicates  $p < 0.01$  and \*\*\* indicates  $p < 0.001$

501

502  
503  
504



505  
506  
507

**Figure A4.** Taxonomic composition of Bacillariophyta at Station 7 based on a) psbA and b) rbcL marker genes. The figure shows the relative abundance of Bacillariophyta genera detected in the metagenomic dataset, grouped by gene-specific classifications.

508

Station	Parameter (X)	Value	SD	$\delta\text{NFR}/\delta X$	Error contribution ( $SD \times [\delta\text{NFR}/\delta X]2$ )	% Total error	Summary (nmol N L <sup>-1</sup> d <sup>-1</sup> )
3	$\Delta t$	1.00	0.00	0.00	0.00	0.00	Mean = 1.13 LOD = 0.73 MQR = 0.12
	$A_{N2}$	3.92%	0.00	0.00	0.00	0.00	
	$A_{PNO}$	0.370%	$4.24 \times 10^{-6}$	$2.63 \times 10^6$	$2.46 \times 10^2$	29.49	
	$A_{PNf}$	0.420%	$3.7 \times 10^{-5}$	$2.36 \times 10^5$	$3.03 \times 10^2$	35.54	
	$[PN]_f$	$1.69 \times 10^3$	$1.24 \times 10^2$	$5.12 \times 10^{-2}$	$3.21 \times 10^2$	34.97	
7	$\Delta t$	1.00	0.00	0.00	0.00	0.00	Mean = 1.92 LOD = 1.91 MQR = 0.47
	$A_{N2}$	3.92%	0.00	0.00	0.00	0.00	

	APNO	0.369%	$4.0 \times 10^{-6}$	$1.57 \times 10^7$	$2.06 \times 10^3$	25.17	
	APNf	0.407%	$5.47 \times 10^{-5}$	$9.25 \times 10^5$	$2.79 \times 10^3$	36.88	
	[PN] <sub>f</sub>	$4.62 \times 10^3$	$8.2 \times 10^2$	$6.77 \times 10^{-2}$	$2.87 \times 10^3$	37.95	
10	$\Delta t$	1.00	0.00	0.00	0.00	0.00	Mean = 0.90 LOD = 0.96 MQR = 0.06
	$A_{N2}$	3.92%	0.00	0.00	0.00	0.00	
	APNO	0.371%	$1.89 \times 10^{-6}$	$-2.01 \times 10^2$	$1.44 \times 10^{-3}$	31.24	
	APNf	0.371%	$2.22 \times 10^{-6}$	$2.01 \times 10^2$	$2.05 \times 10^{-3}$	34.85	
	[PN] <sub>f</sub>	$5.91 \times 10^2$	$1.89 \times 10^2$	$-1.56 \times 10^{-4}$	$3.69 \times 10^{-3}$	33.91	

509 *Table A1: Sensitivity analysis for  $N_2$  fixation rates. The contribution of each source of error to the total uncertainty was determined and*  
 510 *calculated after Montoya et al., (1996). Average values and standard deviations (SD) are provided for all parameters at each station. The*  
 511 *partial derivative ( $\delta NFR/\delta X$ ) of the  $N_2$  fixation rate measurements is calculated for each parameter and evaluated using the provided*  
 512 *average and standard deviation. The total and relative error are given for each parameter. Mean represents the average  $N_2$  fixation rate*  
 513 *measurement. MQR (minimal quantifiable rate) represents the total uncertainty linked to every measurement and is calculated using*  
 514 *standard propagation of error. LOD (limit of detection) represents an alternative detection limit defined as  $\Delta APN = 0,00146$ .*

515  
 516 *Data availability.* The presented data collected during the cruise will be made accessible on PANGEA. The molecular datasets have been  
 517 deposited with the accession number: Bioproject PRJNA1133027

518  
 519  
 520  
 521 *Author contributions.* IS carried out fieldwork and laboratory work at the University of Southern Denmark, and wrote the majority of  
 522 the manuscript. ELP, AM, and EL conducted fieldwork and laboratory work at the University of Southern Denmark. PX performed  
 523 metagenomic analysis and created the corresponding graphs. CRL designed the study, provided supervision and guidance throughout  
 524 the project, and contributed to the writing and revision of the manuscript. All authors contributed to the conception of the study and  
 525 participated in the writing and revision of the manuscript.

526  
 527  
 528  
 529 *Competing interests.* The authors declare that they have no known competing financial interests or personal relationships that could have  
 530 appeared to influence the work reported in this paper. One of the authors, CRL, serves as an Associate Editor for Biogeosciences.

533  
534 *Acknowledgements.* This work was supported by the Velux Foundation (grant no.29411 to Carolin R. Löscher) and through the DFF  
535 grant from the the Independent Research Fund Denmark (grant no. 0217-00089B to Lasse Riemann, Carolin R. Löscher and Stiig  
536 Markager). ELP was supported by a postdoctoral contract from Danmarks Frie Forskningsfond (DFF, 1026-00428B) at SDU, and by a  
537 Marie Skłodowska- Curie postdoctoral fellowship (HORIZON291 MSCA-2021-PF-01, project number: 101066750) by the European  
538 Commission at Princeton University. We sincerely thank the captain and crew of the P540 during the cruise on the Danish military vessel  
539 for their invaluable support and cooperation at sea. Our gratitude extends to Isaaffik Arctic Gateway for providing the infrastructure and  
540 opportunities that made this project possible. We also acknowledge Zarah Kofoed for her technical support in the laboratory and thank all  
541 the Nordceee laboratory technicians for their general assistance.

## 542 **References**

543  
544 Ardyna, M. and Arrigo, K. R.: Phytoplankton dynamics in a changing Arctic Ocean, *Nature Climate Change*, 10, 892–903, 2020.  
545 Ardyna, M., Babin, M., Gosselin, M., Devred, E., Rainville, L., and Tremblay, J.-É.: Recent Arctic Ocean sea ice loss triggers novel fall  
546 phytoplankton blooms, *Geophysical Research Letters*, 41, 6207–6212, 2014.  
547 Arrigo, K. R. and van Dijken, G. L.: Continued increases in Arctic Ocean primary production, *Progress in oceanography*, 136, 60–70,  
548 2015. Arrigo, K. R., van Dijken, G., and Pabi, S.: Impact of a shrinking Arctic ice cover on marine primary production, *Geophysical*  
549 *Research Letters*, 35, 2008.  
550 Arrigo, K. R., van Dijken, G. L., Castelao, R. M., Luo, H., Rennermalm, Å. K., Tedesco, M., Mote, T. L., Oliver, H., and Yager, P. L.:  
551 Melting glaciers stimulate large summer phytoplankton blooms in southwest Greenland waters, *Geophysical Research Letters*, 44,  
552 6278– 6285, 2017.  
553 Bhatia, M. P., Kujawinski, E. B., Das, S. B., Breier, C. F., Henderson, P. B., and Charette, M. A.: Greenland meltwater as a significant  
554 and potentially bioavailable source of iron to the ocean, *Nature Geoscience*, 6, 274–278, 2013.  
555 Blais, M., Tremblay, J.-É., Jungblut, A. D., Gagnon, J., Martin, J., Thaler, M., and Lovejoy, C.: Nitrogen fixation and identification of  
556 potential diazotrophs in the Canadian Arctic, *Global Biogeochemical Cycles*, 26, 2012.  
557 Bonnet, S., Biegala, I. C., Dutrieux, P., Slemmons, L. O., and Capone, D. G.: Nitrogen fixation in the western equatorial Pacific: Rates,  
558 diazotrophic cyanobacterial size class distribution, and biogeochemical significance, *Global Biogeochemical Cycles*, 23, 2009.  
559 Buchanan, P. J., Chase, Z., Matear, R. J., Phipps, S. J., and Bindoff, N. L.: Marine nitrogen fixers mediate a low latitude pathway for  
560 atmospheric CO<sub>2</sub> drawdown, *Nature Communications*, 10, 4611, 2019.  
561 Cantalapiedra, C. P., Hernández-Plaza, A., Letunic, I., Bork, P., and Huerta-Cepas, J.: eggNOG-mapper v2: functional annotation,  
562 orthology assignments, and domain prediction at the metagenomic scale, *Molecular biology and evolution*, 38, 5825–5829, 2021.  
563 Capone, D. G. and Carpenter, E. J.: Nitrogen fixation in the marine environment, *Science*, 217, 1140–1142, 1982.  
564 Chen, Y., Chen, Y., Shi, C., Huang, Z., Zhang, Y., Li, S., Li, Y., Ye, J., Yu, C., Li, Z., et al.: SOAPnuke: a MapReduce acceleration-  
565 supported software for integrated quality control and preprocessing of high-throughput sequencing data, *Gigascience*, 7, gix120, 2018.  
566 Cheung, S., Liu, K., Turk-Kubo, K. A., Nishioka, J., Suzuki, K., Landry, M. R., Zehr, J. P., Leung, S., Deng, L., and Liu, H.: High  
567 biomass turnover rates of endosymbiotic nitrogen-fixing cyanobacteria in the western Bering Sea, *Limnology and Oceanography*  
568 *Letters*, 7, 501– 509, 2022.  
569 Coale, T. H., Loconte, V., Turk-Kubo, K. A., Vanslembrouck, B., Mak, W. K. E., Cheung, S., Ekman, A., Chen, J.-H., Hagino, K.,

571 Takano, Y., et al.: Nitrogen-fixing organelle in a marine alga, *Science*, 384, 217–222, 2024.

572 Dähnke, K. and Thamdrup, B.: Nitrogen isotope dynamics and fractionation during sedimentary denitrification in Boknis Eck, Baltic

573 Sea, *Biogeosciences*, 10, 3079–3088, 2013.

574 Damm, E., Helmke, E., Thoms, S., Schauer, U., Nöthig, E., Bakker, K., and Kiene, R.: Methane production in aerobic oligotrophic

575 surface water in the central Arctic Ocean, *Biogeosciences*, 7, 1099–1108, 2010.

576 Díez, B., Bergman, B., Pedrós-Alió, C., Antó, M., and Snoeijs, P.: High cyanobacterial *nifH* gene diversity in Arctic seawater and sea

577 ice brine, *Environmental microbiology reports*, 4, 360–366, 2012.

578 Emeis, K.-C., Mara, P., Schlarbaum, T., Möbius, J., Dähnke, K., Struck, U., Mihalopoulos, N., and Krom, M.: External N inputs and

579 internal N cycling traced by isotope ratios of nitrate, dissolved reduced nitrogen, and particulate nitrogen in the eastern Mediterranean

580 Sea, *Journal of Geophysical Research: Biogeosciences*, 115, 2010.

581 Falkowski, P. G., Fenchel, T., and Delong, E. F.: The microbial engines that drive Earth's biogeochemical cycles, *science*, 320, 1034–

582 1039, 2008.

583 Farnelid, H., Andersson, A. F., Bertilsson, S., Al-Soud, W. A., Hansen, L. H., Sørensen, S., Steward, G. F., Hagström, Å., and Riemann,

584 L.: Nitrogenase gene amplicons from global marine surface waters are dominated by genes of non-cyanobacteria, *PloS one*, 6, e19 223,

585 2011.

586 Farnelid, H., Turk-Kubo, K., Ploug, H., Ossolinski, J. E., Collins, J. R., Van Mooy, B. A., and Zehr, J. P.: Diverse diazotrophs are present

587 on sinking particles in the North Pacific Subtropical Gyre, *The ISME journal*, 13, 170–182, 2019.

588 Fernández-Méndez, M., Turk-Kubo, K. A., Buttigieg, P. L., Rapp, J. Z., Krumpen, T., and Zehr, J. P.: Diazotroph diversity in the sea ice,

589 melt ponds, and surface waters of the Eurasian Basin of the Central Arctic Ocean, *Frontiers in microbiology*, 7, 217 140, 2016.

590 Foster, R. A., Goebel, N. L., & Zehr, J. P.: Isolation of *calothrix rhizosoleniae* (cyanobacteria) strain SC01 from chaetoceros

591 (bacillariophyta) spp. diatoms of the subtropical north pacific ocean 1. *Journal of Phycology*, 46(5), 1028-1037, 2010.

592 Foster, R. A., Kuypers, M. M., Vagner, T., Paerl, R. W., Musat, N., and Zehr, J. P.: Nitrogen fixation and transfer in open ocean

593 diatom–cyanobacterial symbioses, *The ISME journal*, 5, 1484–1493, 2011.

594 Foster, R. A., Tienken, D., Littmann, S., Whitehouse, M. J., Kuypers, M. M., and White, A. E.: The rate and fate of N2 and C fixation

595 by marine diatom-diazotroph symbioses, *The ISME journal*, 16, 477–487, 2022.

596 Fox, A. and Walker, B. D.: Sources and Cycling of Particulate Organic Matter in Baffin Bay: A Multi-Isotope  $\delta^{13}\text{C}$ ,  $\delta^{15}\text{N}$ , and  $\Delta^{14}\text{C}$

597 Approach, *Frontiers in Marine Science*, 9, 846 025, 2022.

598 Fu, L., Niu, B., Zhu, Z., Wu, S., and Cd-hit, W. L.: Accelerated for clustering the next-generation sequencing data, *Bioinformatics*,

599 28, 3150–3152, 2012.

600 Galloway, J., Dentener, F., Capone, D., Boyer, E., Howarth, R., Seitzinger, S., Asner, G., Cleveland, C., Green, P., Holland, E., et al.:

601 Nitrogen cycles: past, present, and future. *Biogeochemistry* 70, 153e226, 2004.

602 García-Robledo, E., Corzo, A., and Papaspyrou, S.: A fast and direct spectrophotometric method for the sequential determination of

603 nitrate and nitrite at low concentrations in small volumes, *Marine Chemistry*, 162, 30–36, 2014.

604 Geider, R. J., & La Roche, J.: Redfield revisited: variability of C [ratio] N [ratio] P in marine microalgae and its biochemical

605 basis. *European Journal of Phycology*, 37(1), 1-17, 2002.

606 Gladish, C. V., Holland, D. M., and Lee, C. M.: Oceanic boundary conditions for Jakobshavn Glacier. Part II: Provenance and sources

607 of variability of Disko Bay and Ilulissat icefjord waters, 1990–2011, *Journal of Physical Oceanography*, 45, 33–63, 2015.

608 Grosse, J., Bombar, D., Doan, H. N., Nguyen, L. N., & Voss, M.: The Mekong River plume fuels nitrogen fixation and determines  
609 phytoplankton species distribution in the South China Sea during low and high discharge season. *Limnology and*  
610 *Oceanography*, 55(4), 1668–1680, 2010.

611 Großkopf, T., Mohr, W., Baustian, T., Schunck, H., Gill, D., Kuypers, M. M., Lavik, G., Schmitz, R. A., Wallace, D. W., and LaRoche,  
612 J.: Doubling of marine dinitrogen-fixation rates based on direct measurements, *Nature*, 488, 361–364, 2012.

613 Gruber, N.: The dynamics of the marine nitrogen cycle and its influence on atmospheric CO<sub>2</sub> variations, in: The ocean carbon cycle  
614 and climate, pp. 97–148, Springer, 2004.

615 Gruber, N. and Galloway, J. N.: An Earth-system perspective of the global nitrogen cycle, *Nature*, 451, 293–296, 2008.

616 Gruber, N. and Sarmiento, J. L.: Global patterns of marine nitrogen fixation and denitrification, *Global biogeochemical cycles*, 11, 235–  
617 266, 1997.

618 Haine, T. W., Curry, B., Gerdes, R., Hansen, E., Karcher, M., Lee, C., Rudels, B., Spreen, G., de Steur, L., Stewart, K. D., et al.: Arctic  
619 freshwater export: Status, mechanisms, and prospects, *Global and Planetary Change*, 125, 13–35, 2015.

620 Hanna, E., Huybrechts, P., Steffen, K., Cappelen, J., Huff, R., Shuman, C., Irvine-Fynn, T., Wise, S., and Griffiths, M.: Increased runoff  
621 from melt from the Greenland Ice Sheet: a response to global warming, *Journal of Climate*, 21, 331–341, 2008.

622 Hansen, M. O., Nielsen, T. G., Stedmon, C. A., and Munk, P.: Oceanographic regime shift during 1997 in Disko Bay, western  
623 Greenland, *Limnology and Oceanography*, 57, 634–644, 2012.

624 Harding, K., Turk-Kubo, K. A., Sipler, R. E., Mills, M. M., Bronk, D. A., and Zehr, J. P.: Symbiotic unicellular cyanobacteria fix nitrogen  
625 in the Arctic Ocean, *Proceedings of the National Academy of Sciences*, 115, 13 371–13 375, 2018.

626 Hawkins, J., Wadham, J., Tranter, M., Lawson, E., Sole, A., Cowton, T., Tedstone, A., Bartholomew, I., Nienow, P., Chandler, D., et  
627 al.: The effect of warming climate on nutrient and solute export from the Greenland Ice Sheet, *Geochemical Perspectives Letters*, pp.  
628 94–104, 2015.

629 Hawkins, J. R., Wadham, J. L., Tranter, M., Raiswell, R., Benning, L. G., Statham, P. J., Tedstone, A., Nienow, P., Lee, K., and Telling,  
630 J.: Ice sheets as a significant source of highly reactive nanoparticulate iron to the oceans, *Nature communications*, 5, 1–8, 2014.

631 Hendry, K. R., Huvenne, V. A., Robinson, L. F., Annett, A., Badger, M., Jacobel, A. W., Ng, H. C., Opher, J., Pickering, R. A., Taylor, M.  
632 L., et al.: The biogeochemical impact of glacial meltwater from Southwest Greenland, *Progress in Oceanography*, 176, 102 126, 2019.

633 Holland, D. M., Thomas, R. H., De Young, B., Ribergaard, M. H., and Lyberth, B.: Acceleration of Jakobshavn Isbræ triggered by warm  
634 subsurface ocean waters, *Nature geoscience*, 1, 659–664, 2008.

635 Hopwood, M. J., Connelly, D. P., Arendt, K. E., Juul-Pedersen, T., Stinchcombe, M. C., Meire, L., Esposito, M., and Krishna, R.:  
636 Seasonal changes in Fe along a glaciated Greenlandic fjord, *Frontiers in Earth Science*, 4, 15, 2016.

637 Hyatt, D., Chen, G.-L., LoCascio, P. F., Land, M. L., Larimer, F. W., and Hauser, L. J.: Prodigal: prokaryotic gene recognition and  
638 translation initiation site identification, *BMC bioinformatics*, 11, 1–11, 2010.

639 Jensen, H. M., Pedersen, L., Burmeister, A., and Winding Hansen, B.: Pelagic primary production during summer along 65 to 72 N off  
640 West Greenland, *Polar Biology*, 21, 269–278, 1999.

641 Karl, D., Michaels, A., Bergman, B., Capone, D., Carpenter, E., Letelier, R., Lipschultz, F., Paerl, H., Sigman, D., and Stal, L.: Dinitrogen  
642 fixation in the world's oceans, The nitrogen cycle at regional to global scales, pp. 47–98, 2002.

643 Knies, J.: Nitrogen isotope evidence for changing Arctic Ocean ventilation regimes during the Cenozoic, *Geophysical Research Letters*,  
644 49, e2022GL099 512, 2022.

645 Krawczyk, D. W., Yesson, C., Knutz, P., Arboe, N. H., Blicher, M. E., Zinglersen, K. B., and Wagnholt, J. N.: Seafloor habitats across  
646 geological boundaries in Disko Bay, central West Greenland, *Estuarine, Coastal and Shelf Science*, 278, 108 087, 2022.

647 Krupke, A., Mohr, W., LaRoche, J., Fuchs, B. M., Amann, R. I., and Kuypers, M. M.: The effect of nutrients on carbon and nitrogen  
648 fixation by the UCYN-A-haptophyte symbiosis, *The ISME journal*, 9, 1635–1647, 2015.

649 Laso Perez, R., Rivas Santisteban, J., Fernandez-Gonzalez, N., Mundy, C. J., Tamames, J., and Pedros-Alio, C.: Nitrogen cycling during  
650 an Arctic bloom: from chemolithotrophy to nitrogen assimilation, *bioRxiv*, pp. 2024–02, 2024.

651 Lewis, K., Van Dijken, G., and Arrigo, K. R.: Changes in phytoplankton concentration now drive increased Arctic Ocean primary  
652 production, *Science*, 369, 198–202, 2020.

653 Li, D., Liu, C.-M., Luo, R., Sadakane, K., and Lam, T.-W.: MEGAHIT: an ultra-fast single-node solution for large and complex  
654 metagenomics assembly via succinct de Bruijn graph, *Bioinformatics*, 31, 1674–1676, 2015.

655 Löscher, C. R., Bourbonnais, A., Dekaezemacker, J., Charoenpong, C. N., Altabet, M. A., Bange, H. W., Czeschel, R., Hoffmann, C.,  
656 and Schmitz, R.: N<sub>2</sub> fixation in eddies of the eastern tropical South Pacific Ocean, *Biogeosciences*, 13, 2889–2899, 2016.

657 Löscher, C. R., Mohr, W., Bange, H. W., and Canfield, D. E.: No nitrogen fixation in the Bay of Bengal?, *Biogeosciences*, 17, 851–864,  
658 2020. Luo, Y.-W., Doney, S., Anderson, L., Benavides, M., Berman-Frank, I., Bode, A., Bonnet, S., Boström, K. H., Böttjer, D., Capone,  
659 D., et al.: Database of diazotrophs in global ocean: abundance, biomass and nitrogen fixation rates, *Earth System Science Data*, 4, 47–73,  
660 2012.

661 Martínez-Pérez, C., Mohr, W., Löscher, C. R., Dekaezemacker, J., Littmann, S., Yilmaz, P., Lehnen, N., Fuchs, B. M., Lavik, G.,  
662 Schmitz,  
663 R. A., et al.: The small unicellular diazotrophic symbiont, UCYN-A, is a key player in the marine nitrogen cycle, *Nature Microbiology*,  
664 1, 1–7, 2016.

665 Mills, M. M., Turk-Kubo, K. A., van Dijken, G. L., Henke, B. A., Harding, K., Wilson, S. T., Arrigo, K. R., and Zehr, J. P.: Unusual  
666 marine cyanobacteria/haptophyte symbiosis relies on N<sub>2</sub> fixation even in N-rich environments, *The ISME Journal*, 14, 2395–2406,  
667 2020.

668 Mohr, W., Grosskopf, T., Wallace, D. W., and LaRoche, J.: Methodological underestimation of oceanic nitrogen fixation rates, *PloS one*,  
669 5, e12 583, 2010.

670 Montoya, J. P.: Nitrogen stable isotopes in marine environments, *Nitrogen in the marine environment*, 2, 1277–1302, 2008.

671 Montoya, J. P., Carpenter, E. J., and Capone, D. G.: Nitrogen fixation and nitrogen isotope abundances in zooplankton of the oligotrophic  
672 North Atlantic, *Limnology and Oceanography*, 47, 1617–1628, 2002.

673 Mortensen, J., Rysgaard, S., Winding, M., Juul-Pedersen, T., Arendt, K., Lund, H., Stuart-Lee, A., and Meire, L.: Multidecadal water  
674 mass dynamics on the West Greenland Shelf, *Journal of Geophysical Research: Oceans*, 127, e2022JC018 724, 2022.

675 Munk, P., Nielsen, T. G., and Hansen, B. W.: Horizontal and vertical dynamics of zooplankton and larval fish communities during mid-  
676 summer in Disko Bay, West Greenland, *Journal of Plankton Research*, 37, 554–570, 2015.

677 Murphy, J. and Riley, J. P.: A modified single solution method for the determination of phosphate in natural waters, *Analytica chimica  
678 acta*, 27, 31–36, 1962.

679 Myers, P. G. and Ribergaard, M. H.: Warming of the polar water layer in Disko Bay and potential impact on Jakobshavn Isbrae, *Journal  
680 of Physical Oceanography*, 43, 2629–2640, 2013.

681 Patro, R., Duggal, G., Love, M. I., Irizarry, R. A., and Kingsford, C.: Salmon provides fast and bias-aware quantification of transcript  
682 expression, *Nature methods*, 14, 417–419, 2017.

683 Quigg, A., Finkel, Z.V., Irwin, A.J., Rosenthal, Y., Ho, T.Y., Reinfelder, J.R., Schofield, O., Morel, F.M. and Falkowski, P.G.: The  
684 evolutionary inheritance of elemental stoichiometry in marine phytoplankton. *Nature*, 425(6955), pp.291-294, 2003.

685 Redfield, A. C.: On the proportions of organic derivatives in sea water and their relation to the composition of plankton (Vol. 1). Liverpool:  
686 university press of liverpool, 1934.

687 Reeder, C. F., Stoltenberg, I., Javidpour, J., and Löscher, C. R.: Salinity as a key control on the diazotrophic community composition in  
688 the Baltic Sea, *Ocean Science Discussions*, 2021, 1–30, 2021.

689 Rees, A. P., Gilbert, J. A., and Kelly-Gerrey, B. A.: Nitrogen fixation in the western English Channel (NE Atlantic ocean), *Marine  
690 Ecology Progress Series*, 374, 7–12, 2009.

691 Robicheau, B. M., Tolman, J., Rose, S., Desai, D., and LaRoche, J.: Marine nitrogen-fixers in the Canadian Arctic Gateway are  
692 dominated by biogeographically distinct noncyanobacterial communities. *FEMS Microbiology Ecology*, 99(12), 122, 2023.

693 Rysgaard, S., Boone, W., Carlson, D., Sejr, M., Bendtsen, J., Juul-Pedersen, T., Lund, H., Meire, L., and Mortensen, J.: An updated view  
694 on water masses on the pan-west Greenland continental shelf and their link to proglacial fjords, *Journal of Geophysical Research: Oceans*, 125, e2019JC015 564, 2020.

695 Schiøtt, S.: The Marine Ecosystem of Ilulissat Icefjord, Greenland, Ph.D. thesis, Department of Biology, Aarhus University, Denmark,  
696 2023. Schlitzer, R.: Ocean data view, 2022.

697 Schneider, B., Schlitzer, R., Fischer, G. and Nöthig, E.M.: Depth-dependent elemental compositions of particulate organic matter (POM)  
698 in the ocean. *Global Biogeochemical Cycles*, 17(2), 2003.

699 Schvarcz, C. R., Wilson, S. T., Caffin, M., Stancheva, R., Li, Q., Turk-Kubo, K. A., White, A. E., Karl, D. M., Zehr, J. P., and Steward, G.  
700 F.: Overlooked and widespread pennate diatom-diazotroph symbioses in the sea, *Nature communications*, 13, 799, 2022.

701 Shao, Z., Xu, Y., Wang, H., Luo, W., Wang, L., Huang, Y., Agawin, N. S. R., Ahmed, A., Benavides, M., Bentzon-Tilia, M., et al.:  
702 Global oceanic diazotroph database version 2 and elevated estimate of global N 2 fixation, *Earth System Science Data*, 15, 2023.

703 Sherwood, O. A., Davin, S. H., Lehmann, N., Buchwald, C., Edinger, E. N., Lehmann, M. F., and Kienast, M.: Stable isotope ratios in  
704 seawater nitrate reflect the influence of Pacific water along the northwest Atlantic margin, *Biogeosciences*, 18, 4491–4510, 2021.

705 Shiozaki, T., Bombar, D., Riemann, L., Hashihama, F., Takeda, S., Yamaguchi, T., Ehama, M., Hamasaki, K., and Furuya, K.: Basin  
706 scale variability of active diazotrophs and nitrogen fixation in the North Pacific, from the tropics to the subarctic Bering Sea, *Global  
707 Biogeo- chemical Cycles*, 31, 996–1009, 2017.

708 Shiozaki, T., Fujiwara, A., Ijichi, M., Harada, N., Nishino, S., Nishi, S., Nagata, T., and Hamasaki, K.: Diazotroph community structure  
709 and the role of nitrogen fixation in the nitrogen cycle in the Chukchi Sea (western Arctic Ocean), *Limnology and Oceanography*, 63,  
710 2191–2205, 2018.

711 Shiozaki, T., Fujiwara, A., Inomura, K., Hirose, Y., Hashihama, F., and Harada, N.: Biological nitrogen fixation detected under Antarctic  
712 sea ice, *Nature geoscience*, 13, 729–732, 2020.

713 Shiozaki, T., Nishimura, Y., Yoshizawa, S., Takami, H., Hamasaki, K., Fujiwara, A., Nishino, S., and Harada, N.: Distribution and  
714 survival strategies of endemic and cosmopolitan diazotrophs in the Arctic Ocean, *The ISME journal*, 17, 1340–1350, 2023.

715 Sigman, D. M., DiFiore, P. J., Hain, M. P., Deutsch, C., Wang, Y., Karl, D. M., Knapp, A. N., Lehmann, M. F., and Pantoja, S.: The  
716 dual isotopes of deep nitrate as a constraint on the cycle and budget of oceanic fixed nitrogen, *Deep Sea Research Part I: Oceanographic  
717 Research Papers*, 56, 1419–1439, 2009.

718 Sipler, R. E., Gong, D., Baer, S. E., Sanderson, M. P., Roberts, Q. N., Mulholland, M. R., and Bronk, D. A.: Preliminary estimates of

720 the contribution of Arctic nitrogen fixation to the global nitrogen budget, Limnology and Oceanography Letters, 2, 159–166, 2017.

721 Slawyk, G., Collos, Y., and Auclair, J.-C.: The use of the  $^{13}\text{C}$  and  $^{15}\text{N}$  isotopes for the simultaneous measurement of carbon and nitrogen

722 turnover rates in marine phytoplankton 1, Limnology and Oceanography, 22, 925–932, 1977.

723 Sohm, J. A., Webb, E. A., and Capone, D. G.: Emerging patterns of marine nitrogen fixation, Nature Reviews Microbiology, 9, 499–

724 508, 2011.

725 Sterner, R. W., & Elser, J. J. Ecological stoichiometry: the biology of elements from molecules to the biosphere. In Ecological stoichiometry.

726 Princeton university press, 2017.

727 Tanioka, T., Garcia, C.A., Larkin, A.A., Garcia, N.S., Fagan, A.J. and Martiny, A.C.: Global patterns and predictors of C: N: P in marine

728 ecosystems. Communications Earth & Environment, 3(1), p.271, 2022.

729 Tang, W., Wang, S., Fonseca-Batista, D., Dehairs, F., Gifford, S., Gonzalez, A. G., Gallinari, M., Planquette, H., Sarthou, G., and Cassar,

730 N.: Revisiting the distribution of oceanic  $\text{N}_2$  fixation and estimating diazotrophic contribution to marine production, Nature

731 communications, 10, 831, 2019.

732 Tremblay, J.-É. and Gagnon, J.: The effects of irradiance and nutrient supply on the productivity of Arctic waters: a perspective on

733 climate change, in: Influence of climate change on the changing arctic and sub-arctic conditions, pp. 73–93, Springer, 2009.

734 Turk, K. A., Rees, A. P., Zehr, J. P., Pereira, N., Swift, P., Shelley, R., Lohan, M., Woodward, E. M. S., and Gilbert, J.: Nitrogen fixation

735 and nitrogenase (*nifH*) expression in tropical waters of the eastern North Atlantic, The ISME journal, 5, 1201–1212, 2011.

736 Turk-Kubo, K. A., Frank, I. E., Hogan, M. E., Desnues, A., Bonnet, S., and Zehr, J. P.: Diazotroph community succession during the

737 VAHINE mesocosm experiment (New Caledonia lagoon), Biogeosciences, 12, 7435–7452, 2015.

738 Von Friesen, L. W. and Riemann, L.: Nitrogen fixation in a changing Arctic Ocean: an overlooked source of nitrogen?, Frontiers in

739 Microbiology, 11, 596 426, 2020.

740 Wang, S., Bailey, D., Lindsay, K., Moore, J., and Holland, M.: Impact of sea ice on the marine iron cycle and phytoplankton productivity,

741 Biogeosciences, 11, 4713–4731, 2014.

742 Zehr, J. P. and Capone, D. G.: Changing perspectives in marine nitrogen fixation, Science, 368, eaay9514, 2020.